# Acclimation of Endosymbiotic Symbiodiniaceae:

# Improved Insights through Flow Cytometric Phenotypic Profiling

By
**Colin Jeffrey Anthony**

A thesis submitted in partial fulfillment of the
requirements for the degree of

**Master of Science:**
**Biology**

**Supervisory Committee**
Dr. Bastian Bentlage
Dr. Brett M Taylor
Dr. Cheryl Lewis Ames

**University of Guam**
May 2023

**Abstract**

Coral-associated dinoflagellates (Family Symbiodiniaceae) play a vital role in both long-term and short-term survival. The successful acclimation and adaptation of these endosymbionts can be facilitated by changes in the community, population or individual depending on the magnitude and type of stressor or environmental change. However, characterizing all levels of change can be difficult. Therefore, I developed a protocol to generate phenotypic profiles of individual Symbiodiniaceae using a benchtop flow cytometer. Once the protocol was well developed, 20 GPS-tagged colonies across five reef flats around Guam were repeatedly sampled at key temporal points allowing for the paired quantification of assemblage phenotypic variance, at the individual, population, and community level. Symbiodiniaceae assemblages displayed site and season-specific phenotypic signatures, while community composition and cell densities in host tissues remained temporally stable. Symbiodiniaceae biodiversity was relatively low, yet it displayed distinct geographic organization. Additionally, cell density and biodiversity had no correlation to phenotypic variance. Therefore, I hypothesize phenotypic plasticity is the primary mode of acclimation to mild environmental change, while changes in biodiversity are a form of long-term assemblage adaptation after acute selective events or chronic environmental pressures.

**Keywords:** *coral reefs, symbiosis, photosynthesis, acclimation, adaptation*

**Acknowledgements**

There is a countless number of people that have contributed to the work included here as well as work otherwise associated with my time at the University of Guam; however, I must specifically thank research associate Colin Lock*. He has contributed countless hours to the development of these ideas, and I look forward to our continued work together. Additionally I must thank the supervisory committee associated with this thesis: Dr. Bastian Bentlage*, Dr. Brett Taylor*, and Dr. Cheryl Ames*. All three professors provided me the creative freedom to focus on what I found interesting, as I found it interesting, preventing burnout and promoting an environment where I felt my personal development was more important than my productivity, which ironically lead me to be more motivated and productive. I would recommend any of these professors to any student at any time. Most of our conversations were about culture, jellyfish, politics, life, and not coral; I wouldn't have it any other way. While not formally associated with this thesis, other friends and coworkers that contributed substantial intellectual and emotional support included: Benjamin Deloso, Star Dressler, Jessica Fernandez, Naotaka Fukano, MacKenzie Heagy*, Dr. Rebecca Helm*, Ka'ohinani Kawahigashi, Khanh Ly, Dr. Shinichiro Maruyama, Andrew McInnis*, Therese Miller, Dr. Matthew Mills*, Juan-Carlos Mungaray, Loreto Paulilno, Jr., Jonathan "Nanny" Perez, Adam Perez*, Dr. Laurie Raymundo, Dr. Héloïse Rouzé*, Rebecca Salas, Dr. Gaurav Shimpi, Kei Chloe Tan, and Abram Townsend.

*An extra thank you

**Funding**

The entirety of this thesis was funded by NSF Guam EPSCoR: GECCO (OIA-1946352).

**Table of Contents**

**Chapter 2:** Spatio-Temporal Acclimation and Adaptation of the Symbiodiniaceae Assemblages Associated with Guam's Dominant Staghorn Coral *Acropora pulchra*

## 2.5 Conclusions

## 2.6 Acknowledgments

## 2.7 References

**List of Tables**

**List of Figures**

**Figure 2.4.** ITS2 type diversity and ITS2 type profiles from spatio-temporal sampling across five sites (North, Northwest, West, South, and East) and two timepoints (May and August).

**Figure 2.5**. Cell density and phenotype variance visualized as boxplots (Site * Season) and Tuft's boxplots (Plot * Site * Season).

**Figure 2.6.** Three-dimensional dot plots visualizing phenotypic profiles for North, Northwest, West, South, and East Symbiodiniaceae assemblages across repeated temporal sampling (May & August).

**Figure 2.7.** Cell density and phenotypic measurements were mapped to samples with successfully identified ITS2 type profiles.

**Figure 2.8.** Colonies in different sites demonstrated different levels of pigmentation not only from each other, but also across seasons, as demonstrated by repeated photographs during May and August of the same colonies from the North and East sites.

# Chapter 1

# High-throughput physiological profiling of endosymbiotic dinoflagellates (Symbiodiniaceae) using flow cytometry

## 1.0 Summary

Endosymbiotic dinoflagellates (Family Symbiodiniaceae) are directly responsible for coral survival during climate change, as the breakdown of the coral-dinoflagellate symbiosis leads to coral bleaching and often mortality. Despite methodological progress, assessing the physiology of Symbiodiniaceae *in-hospite* remains a complex task. Bio-optics, biochemistry, or "-omics" techniques are expensive, often inaccessible to investigators, or lack the resolution required to understand single-cell physiological states within endosymbiotic dinoflagellate assemblages. To help address this issue, I developed a protocol that generates a physiological profile of Symbiodiniaceae cells while simultaneously determining cell densities using an entry-level benchtop flow cytometer. Two excitation/emission profiles in the red spectrum target light harvesting complex (LHC)-associated pigments, while green and yellow autofluorescence provides insight into antioxidant-associated pigments. Excitation/emission profiles are generated for each individual cell, simultaneously profiling thousands of Symbiodiniaceae cells, thus increasing statistical power to discriminate between groups even when effect sizes are small. As flow cytometry is adopted as a robust and efficient method for endosymbiont cell counting, integration and expansion of our protocol into existing workflows allows quantification of endosymbiont photophysiology and stress-signatures with minimal additional effort.

## 1.1 Introduction

Symbiodiniaceae are dinoflagellates known for their endosymbiotic relationship with many marine invertebrates, most notably reef building corals (LaJeunesse et al., 2018). The breakdown of this symbiosis can lead to coral bleaching and mortality (Hoegh-Guldberg 1999). Despite methodological progress identifying functional and genetic variation in Symbiodiniaceae, assessing trait variation of Symbiodiniaceae *in hospite* remains a complex task (Davies et al., 2022). Pulse Amplitude Modulated (PAM) fluorometry is widely used to quantify photosynthetic efficiency of Symbiodiniaceae photosystems *in hospite* (Warner et al. 1996) both *in situ* (e.g. Suwa et al. 2008) and *ex situ* (e.g. Berg et al. 2021). However, PAM fluorometry provides an aggregate measure of photosystem performance for the Symbiodiniaceae population and does not quantify variation in photosystem performance between cells within the symbiont population. Isolation, characterization, and quantification of photopigments is laborious and time consuming, relying on the extraction of pigments from cells prior to analysis, followed by the normalization of measured pigment quantities to observed cell densities or overall protein content (e.g. Hennige et al. 2009; Fernandes de Barros Marongoni et al. 2020). By contrast, flow cytometry has been demonstrated as a rapid method to quantify algal photopigments and requires comparatively little sample preparation.

Flow cytometry was developed in 1968 (Dittrich and Göhde 1973) and has experienced massive advances in the last 50 years moving from simply counting cells to detecting fluorescent protein markers, detecting RNA expression, describing cell cycles by staining DNA, studying signal pathways with antibodies, sorting cells, and quantifying protein content with fluorescent tags (reviewed in McKinnon 2018). Within coral biology, flow cytometry is widely used for determining Symbiodiniaceae cell density (e.g., Krediet et al. 2015), but can also identify

functional groups of Symbiodiniaceae (Apprill et al. 2007; McIlroy et al. 2014; McIlroy et al. 2020), quantify autofluorescent pigments (Lesser 1996; Lee et al. 2012), enumerate bacterial communities (Patten et al. 2006; Batteral et al. 2016), and even examine cell cycle dynamics (Fujise et al. 2018; Tivey et al. 2020; Figuero et al. 2021). In 1983, a couple groups highlighted the power of flow cytometry for phytoplankton research, demonstrating its ability to characterize phytoplankton communities with taxonomic, optical (pigmentation), and size-based descriptions (Yentsh et al. 1983; Olsen et al. 1983; Cunningham 1993; Sosik et al. 2010). Somewhat lesser known is flow cytometry's ability to rapidly quantify fluorescent photopigments by measuring the relative strength of their fluorescent signal (Olsen et al. 1983; Lesser 1996; Dubelaar and Jonker 2000; Becker et al. 2002; Lee et al. 2012; Chen et al. 2017), which has been validated multiple times by comparing patterns against more robust photopigment quantification methodologies (e.g. LCMS) (Becker et al. 2002; Freitas et al. 2014; Chen et al. 2017). Measuring photopigments with flow cytometry is an extremely rapid estimate of photopigment content and is the only method to our knowledge capable of simultaneously quantifying cellular pigment and biovolume.

Flow cytometry has high potential for the rapid characterization of endosymbiotic Symbiodiniaceae communities; however, it is important for researchers to thoroughly recognize biases, sensitivity resolution, and limitations. Relative data resolution requires high preparation consistency and knowledge of your system. Despite this, I found no thorough protocols or even discussions considering Symbiodiniaceae-specific photopigments, sample preservation, batch effects, and degradation. I identify this as a substantial literature gap given the increasing popularity of flow cytometry in coral biology. To help address these issues, I developed and demonstrated an in-depth protocol for simultaneously quantifying Symbiodiniaceae cell densities and physiological profiles. This research not only includes a detailed protocol but provides an

example framework for implementing it within your workflows, sample analysis with empirical data, and additional theoretical applications. Our protocol takes advantage of flow cytometry's high-throughput nature to generate multivariate physiological profiles for individual cells. With proper implementation and limitation considerations, I hypothesize that this protocol may be used to identify functional differences in Symbiodiniaceae assemblages between host species, sampling sites, timepoints, and even potentially identify niche partitioning of Symbiodiniaceae populations within a single host.

## 1.2 Materials and Methods

***1.2.1 Protocol.*** The protocol described in this article was developed using the Guava easyCyte 6HT-2L (Luminex Corporation, Austin, TX) benchtop flow cytometer and is available through protocols.io (https://dx.doi.org/10.17504/protocols.io.dm6gpjr2jgzp/v2).

***1.2.2 Inferring autofluorescence targets.*** Our flow cytometry protocol relies on two excitation lasers (blue and red) and emission detectors in the green, yellow, and red spectra. Excitation-emission profiles used are as follows: (1) red fluorescence (695/50 nm) off the blue (488 nm) excitation laser (RED-B), (2) red fluorescence (661/15 nm) off of the red (642 nm) excitation laser (RED-R), (3) green fluorescence (525/30 nm) and (4) yellow fluorescence (583/26 nm) off the blue (488 nm) excitation laser (GRN-B and YEL-B respectively). In other flow cytometry methods, researchers typically compensate for spillover and spectral overlap by using labeled antibodies as controls to compensate out cellular autofluorescence and other contaminating fluorophores. This makes sense when using cytometry to detect labeled cellular structures (e.g. induction of labeled proteins through heat shock). However, quantifying autofluorescence requires different techniques given the high protein diversity and spectral overlap. By identifying all possible targets within Symbiodiniaceae (c.f. Venn et al. 2006; Koziol et al. 2007; Hennige et al.

2009; Mukherjee et al. 2013) and modeling their excitation and emission profile based on previously published literature (e.g. Zapata et al. 2001; Yacobi 2012; Koyama and Hashimoto 1993; Kagatani et al. 2022), I can infer our targets.

Symbiodiniaceae autofluorescence signatures are dominated by photosynthetic pigments such as chlorophylls and carotenoids. Excitable pigments previously identified from Symbiodiniaceae include beta-carotene, chlorophylls *a* and $c_2$, diadinoxanthin, diatoxanthin, and peridinin (Venn et al. 2006; Hennige et al. 2009). I also identified flavin-based fluorescent proteins (FbFPs) as a probable source of autofluorescence (Koziol et al. 2007; Mukherjee et al. 2013). To model our autofluorescence targets and identify any risk of spectral overlap, spectral properties of chl *a* and riboflavin (FbFPs), compensated for blue (488 nm) and red (642 nm) laser excitation, were visualized using FluoroFinder Spectra Viewer (https://app.fluorofinder.com/ffsv/svs/). Peridinin, beta-carotene (Koyama and Hashimoto 1993), diadinoxanthin (Kagatani et al. 2022) and chl $c_2$ (Zapata et al. 2001; Yacobi 2012) spectra were mapped to each other using the FluoroFinder spectra and absorbance spectra from Bricaud et al. (2004).

***1.2.3 Optimization assays.*** Two simple assays were designed and performed to provide a framework for optimizing the protocol when integrating it into your own local workflows. In both optimization assays, ideal conditions (temperature, dilution, time, etc.) were selected based on fluorescent distributions with the highest consistency and tightest variances. This included FSC (cell size) and SSC (cell roughness) to detect potential cell clumping and cell lysing, respectively (Mullaney et al. 1969; Steen 1980; Watson 1991; Shapiro 2003; Tzur et al. 2011).

(1) Assay one was used to determine the impacts of time, temperature, and light conditions on samples and the resulting data. A single staghorn coral (*Acropora pulchra*) fragment was

airbrushed with filtered, sterile seawater to create a 30 mL (~150,000 cells/mL) tissue slurry. The slurry was homogenized by vortexing and needle shearing, then equally distributed across four 50 mL falcon tubes. One mL of the tissue slurry was aliquoted from each falcon tube and immediately processed using our cytometry protocol (Anthony et al. 2022a). After aliquots were removed, falcon tubes were separated and exposed to one of four conditions: (1) dark on ice, (2) dark at room temperature (22℃), (3) ambient light on ice, and (4) ambient light at room temperature. A 1 mL sample from each falcon tube was processed approximately every two hours for a total of eight hours; a final set of samples was processed after being stored in their respective conditions overnight. This yielded six temporal samples processed 43, 136, 236, 344, 470, and 1459 minutes after removing tissue from the skeleton. At each time point, treatment replicates were loaded across three wells, and each well was sampled by the flow cytometer twice, creating six technical replicates per sample replicate.

(2) Assay two was used to optimize tissue slurry dilutions and to identify possible effects of flow cytometer run times. I prepared six 1 mL (~150,000 cells/mL) tissue slurries from a single *Acropora pulchra* fragment for flow cytometry using our protocol (Anthony et al. 2022a). Before loading samples into a 96-well microwell plate, all processed tissue slurries were combined into a single 50 mL falcon tube, needle sheared, and vortexed to homogenize samples to avoid possible batch effects. 50x, 20x, 10x, 5x, 2x, and 1x dilutions of the combined tissue slurry were prepared directly in the 200 uL wells. This created a total of 16 dilution series replicates, filling all 96 wells of the plate. Each replicate dilution (2 technical replicates) was processed at ~5 min intervals until the run was complete.

***1.2.4 Example Application.*** In addition to the optimization assays, I also perform a simple acclimation experiment with the upside-down jellyfish *Cassiopea* to highlight the diversity of

hosts the protocol can process, demonstrate data handling techniques, and discuss possible interpretations. Clonal *Cassiopea* were placed into three different conditions for three weeks, each. Prior to the start of the experiment, clonal *Cassiopea* were cultured at UnderWater World® in Tumon, Guam. *Cassiopea* were then transferred to flow through tanks on April 1, 2022, at the University of Guam Marine Laboratory in Mangilao Guam and allowed to acclimate until the start of the experiment on June 8, 2022. All jellyfish were 55-79 mm in diameter at the start of the experiment. Group 1 (n=4) was placed in low-light conditions (50% shade), group 2 in high-light conditions (no shade) (n=4), and group 3 experienced variable environmental conditions (n=5) rotating from high-light to low-light to high-light (one week per condition). At the end of three weeks, digitate ciri (clusters of tentacle-like structures attached to the top of each oral arm (c.f. Anthony et al. 2022b)) were sampled with sterile scissors from each individual and placed in 1 mL of filtered seawater. Symbiodiniaceae cells were subsequently extracted and processed following our flow cytometry protocol (Anthony et al. 2022a).

After identifying the Symbiodiniaceae cells based on red autofluorescence (RED-B) (Figure 2.1), particulate noise was removed from the dataset (RED-B-HLog < 3.04001) yielding sample sizes of 16,134, 18,464, and 19,821 single-cell fluorescent profiles, independent of host, for dark, light, and variable treatment groups, respectively. To better understand effect size and statistical power differences, data was analyzed at two resolutions: dinoflagellate (n=16,134, 18464, 19,821) and host (n = 4, 4, 5). At both resolutions treatment groups were compared by using non-parametric Kruskal-Wallis tests ($X^2$) followed by post-hoc pairwise Dunn's tests (Z) using the FSA R package v0.9.3 (Ogle et al. 2022). All data processing and analysis was completed with R v4.1.2 (R Core Team 2021) in RStudio v1.3.1073 (RStudio Team 2020). Code for this analysis has been deposited on a public GitHub repository with the necessary input files

(https://github.com/AnthonyCuog/CytometryProtocol). Figures were generated and modified with a combination of ggplot2 v3.3.5 (Wickham 2016) and InkScape v1.1 (https://inkscape.org).

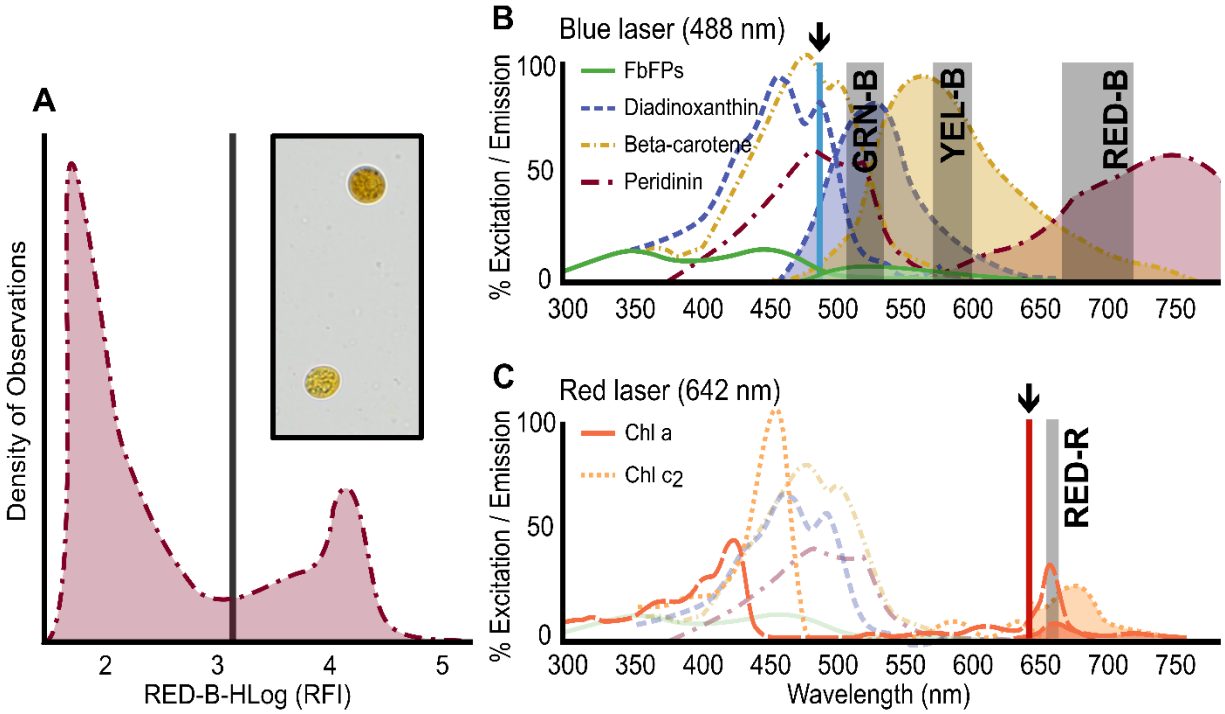


**Figure 1.1. A**) Symbiodiniaceae cells are identified with the RED-B laser profile based on their red fluorescence. **B-C**) Excitation/emission spectra employed by the flow cytometry protocol presented in this contribution. Excitation laser wavelengths are indicated by arrows. Lines depict absorption spectra, while lines with shaded areas illustrate compensated emission wavelengths based on the corresponding excitation laser. **B**) The blue laser (488 nm) simultaneously excited FbFPs, diadinoxanthin, beta-carotene, and peridinin, but emission filters helped identify seperate pigments (**grey boxes**) **C**) The red laser (642 nm) excited chl *a* and chl $c_2$ with a bias towards chl $c_2$.

## 1.3 Results

***1.3.1 Fluorescent pigment identification.*** Red light emission caused by excitation with a blue laser (RED-B) represents the core light harvesting complex (LHC) pigment peridinin (Supasri et al., 2021; Kawalska et al., 2013; Jiang et al., 2012; Bujak et al., 2009). Despite some risk of spectral overlap by beta-carotene, the strong favoritism for peridinin supports this identification (Figure 1.1B). Additionally, spectral plots indicate that red light emission caused by excitation with the red laser (RED-R) represents a combined emission/excitation signature of chlorophyll *a* and

chlorophyll $c_2$ (chl *a* & chl $c_2$) (Niedzwiedzki et al., 2014; Scheer, 2006). Despite the suboptimal excitation wavelength (642 nm), the red laser indicates no risk of spectral overlap from other fluorescent targets, it simply cannot distinguish between different chlorophyll species (Figure 1.1C).

Increased green fluorescence in dinoflagellates under stress has been attributed to beta-carotene (Lee et al., 2012; Kleinegris et al., 2010). However, diadinoxanthin, diatoxanthin (Kagatani et al. 2022; Frank et al. 1996), and flavin-based fluorescent proteins (FbFPs) (Mukherjee et al. 2013; Koziol et al. 2007; Fujita et al. 2005) also emit green fluorescent light when excited by blue light (Figure 1.1B). Therefore, I inferred that both GRN-B and YEL-B represent the combined signature of beta-carotene, xanthophylls (diadinoxanthin and diatoxanthin), and flavins due to fluorescent target spectral overlap (Figure 1.1B).

***1.3.2 Effects of sample preparation on degradation.*** Samples stored on ice and processed within approximately two hours (136 minutes) showed the most consistent signatures across all measurements (Figure 1.2). RED-B and RED-R autofluorescence degraded relatively quickly at ambient temperatures, but light exposure alone does not appear to have a strong effect (Figs 1.2A-B). GRN-B remained stable during the first two hours, regardless of treatment, but variability increased after longer incubation (Figure 1.2C). Interestingly, cell concentrations were more stable under ambient temperatures but still produced consistent results when processed within 136 minutes after being stored on ice (Figure 1.2D).

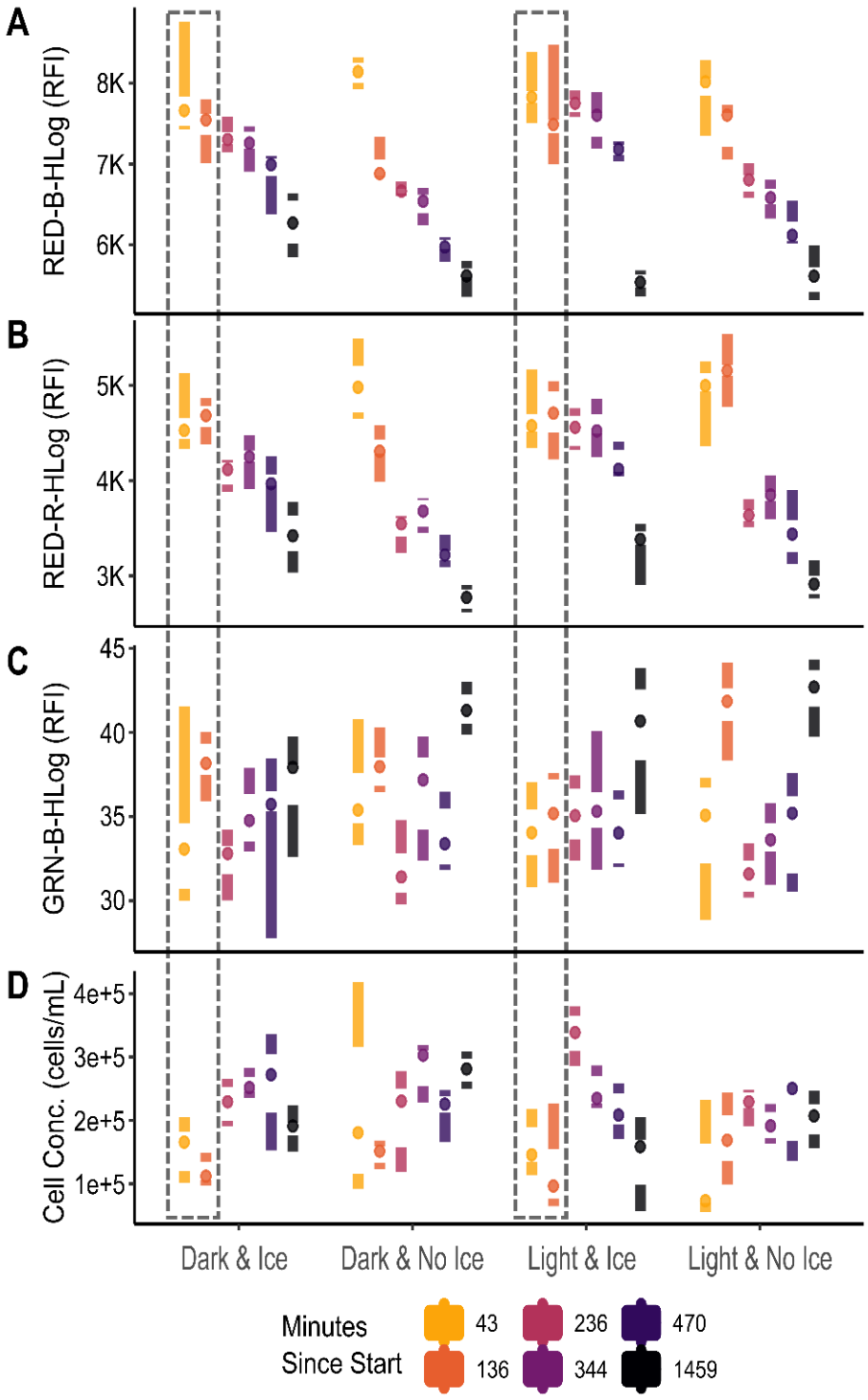


**Figure 1.2.** Samples prepared under different light (Dark vs Light) and temperature (Ice vs No Ice) conditions produced different parameter estimates. Only samples processed on ice within roughly two hours (136 minutes) of airbrushing yielded consistent results (**dashed boxes**). RED-B (**A**) and RED-R (**B**) autofluorescence degraded quickly, but GRN-B (**C**) remained relatively stable over time. Interestingly, cell concentrations (**D**) were more stable under ambient conditions (no ice) but produced relatively consistent results when processed within 136 minutes after being stored on ice.

***1.3.3 Effects of dilution and flow cytometer run-time on degradation.*** Six dilutions (50x, 20x, 10x, 5x, 2x, and 1x) were tested 16 times each across a 96-well plate resulting in individual sample measurements of ~150,000 cells/mL for each replicate (Figure 1.3). The flow cytometer run took around six hours to complete. Ten-fold and five-fold dilutions in the first four rows of the 96-well plate were the most consistent. More diluted samples produced unstable means of measured parameters, while less diluted samples exacerbated degradation. RED-B fluorescence degraded with time (Figure 1.3A), while RED-R, GRN-B, and YEL-B fluorescence increased with time (Figure 1.3B-D). Cell size (forward scatter) did not show any effects of degradation, but highly concentrated samples over estimated size, likely due to cell clumping (Figure 1.3E). Cell roughness (side scatter) is the most stable metric suggesting low rates of cell lysis, though increasing quartile ranges in the one-fold and two-fold dilutions suggest increased susceptibility to lysis in higher concentrations (Figure 1.3F). Estimates of cell concentrations were heavily affected by dilution and run-time (Figure 1.3G).

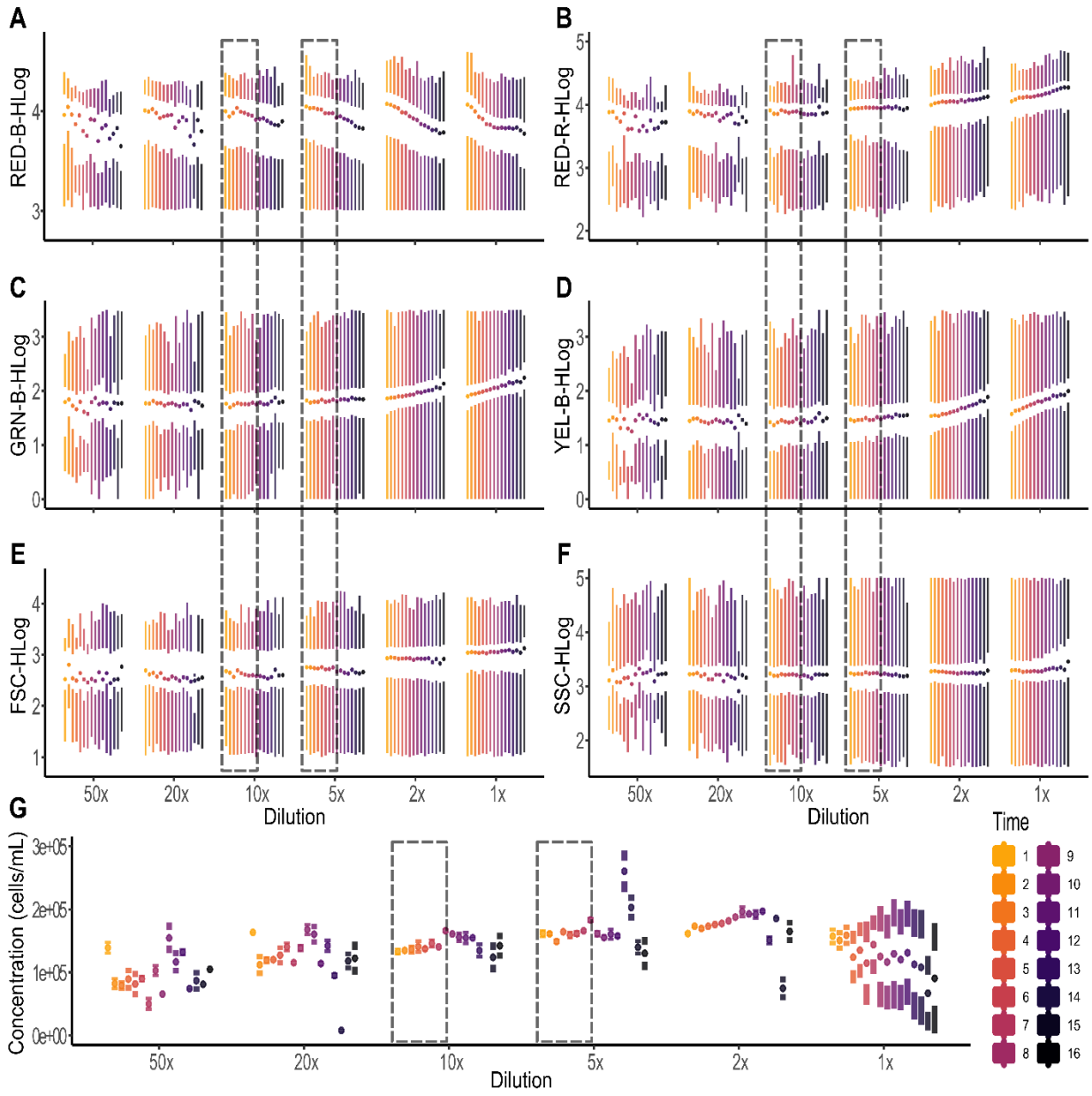


**Figure 1.3.** Six dilutions (50x, 20x, 10x, 5x, 2x, and 1x) were tested 16 times each across a 96-well plate. The cytometry run took ~6 hours estimating ~20 minutes between each of the 16 replicates (**Time**). Ten-fold and five-fold dilutions were the most consistent for half of the plate (**dashed boxes**) suggesting that runs should be limited to ≤ 48 wells (half of a standard 96-well plate). Over- or under-dilution of samples had a large effect on resulting parameter estimates. **A**) RED-B (peridinin) fluorescence degraded over time and had more variation with 50x and 20x dilutions. **B-D**) RED-R, GRN-B, and YEL-B fluorescence increased over time, presumably due to heat generated by the flow cytometer. **E**) Cell size (FSC) did not change over time, but highly concentrated samples led to an overestimation of cell sizes, likely due to cell clumping. **F**) Cell roughness (SSC) was the most stable parameter, suggesting low rates of cell lysis. **G**) Cell concentrations were heavily affected by dilution and time spent in the flow cytometer.

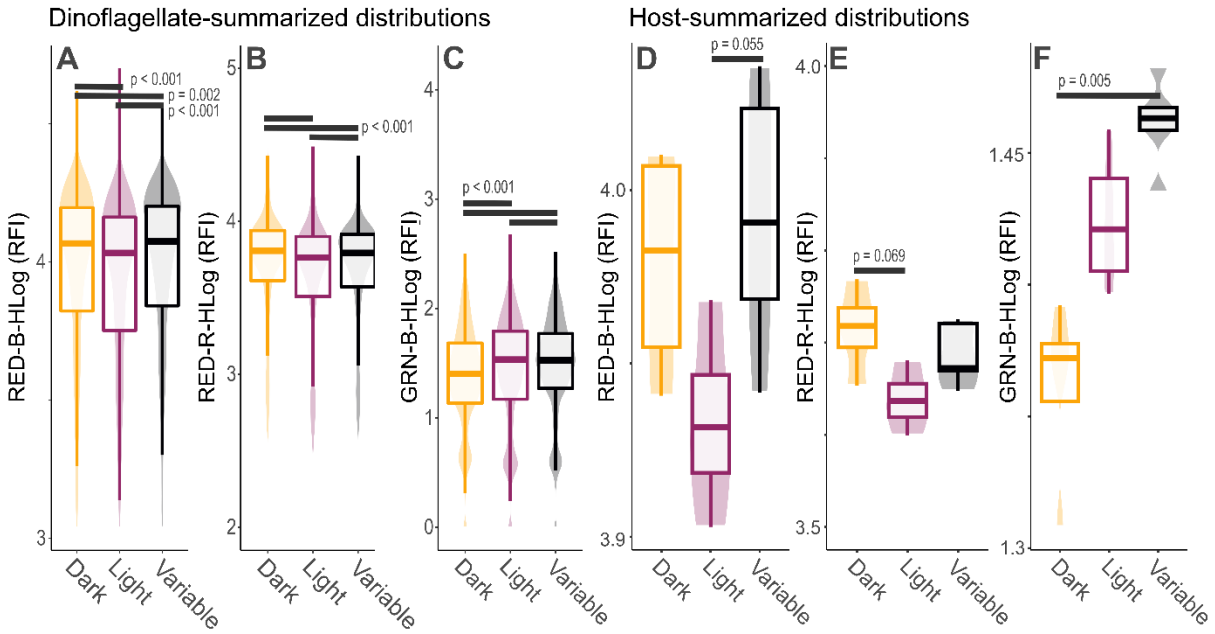


**Figure 1.4.** Digitate cirri from the upside-down jellyfish, *Cassiopea* sp., were sampled and processed with our flow cytometry protocol (S1 File) after three weeks of exposure to different light conditions. **A-C**) Each pairwise comparison indicated statistically significant differences in means ($p < 0.01$); the most distinct distribution ($p < 0.001$) is indicated by "***". Each distribution represents 16,000 - 20,000 observations, which allowed for discriminating between treatments, even with small effect size. **D-F**) Cellular fluorescence averaged to the jellyfish host better illustrates the acclimation pattern with less statistical power ($p = 0.005$ to 0.069).

***1.3.4 Upside-down jellyfish light acclimation experiment.*** After three weeks, *Cassiopea* medusae visibly changed color with dark-acclimated individuals being dark brown and light-acclimated individuals being light browwn. The treatment influenced fluorescent readings for all excitation/emission parameters, but statistical power varied between different resolutions (dinoflagellate vs. host) (Figure 1.4). Light-acclimated individuals had the lowest peridinin (RED-B) and chl *a* & $c_2$ (RED-R) signals, while dark-acclimated individuals had the lowest green emission signal ('antioxidant' pigments) (Figure 1.4). When all cell-specific measurements within each treatment were included in distributions (Figure 1.4A-C), Dunn's pairwise comparisons demonstrated a difference in means ($p \leq 0.002$), despite a small effect size. The only comparison with an adjusted p-value greater than 0.001 was the dark vs variable RED-B comparison ($p =$

0.002). Alternatively, when summarizing flow cytometry data to the cnidarian host, statistics were less powerful, while treatment effect became more conspicuous (Figure 1.4D-F).

## 1.4 Discussion

***1.4.1 Photopigments and autofluorescence signatures.*** Understanding Symbiodiniaceae-specific photosynthetic structures could influence data interpretation. Symbiodiniaceae does not have chlorophyll *b* (Venn et al. 2006; Hennige et al. 2009), a very common chlorophyll molecule in other photosynthetic organisms that would normally be detected by our laser/filter combinations. Instead, Symbiodinaceae possess two major LHC antennae, the peridinin-chlorophyll *a* protein complex (PCP) and the chlorophyll *a*-chlorophyll $c_2$-peridinin protein complex (acpPC), which use peridinin and chl $c_2$ as the primary light-harvesting pigments (Polívka et al. 2007; Hiller et al. 1993). This is then used to form physiological hypotheses. For example, based on our modeled excitation/emission spectra, our laser profiles most likely separate peridinin (RED-R) and chlorophylls (RED-B) quite well (Figure 1.1); despite the risk of beta-carotene spilling into the peridinin reading (Figure 1.1B). However, in Lesser 1996, red fluorescence (630 nm long-pass filters) measured off a 488 nm excitation laser, the same excitation laser used here, was identified as chlorophyll, despite no citation for identification. Our plotted spectra indicate Lesser (1996) was more likely detecting peridinin or even beta-carotene given the lower spectral emission filter used (Figure 1.1B). The exact identity of these red fluorescent signatures remains to be resolved; however, peridinin's tight association with chlorophylls in LHC antennae (Kanazawa et al. 2014; Jiang et al. 2012; Schulte et al. 2010; Polívkaa et al. 2007; Hiller et al. 1993) means the interpretation remains largely the same. A conservative interpretation of our *Cassiopea* acclimation experiment (Figure 1.4) could be as follows: The reduction of red fluorescent intensity in high light indicates the downregulation of photosynthetic pigments within Symbiodiniaceae

cells to reduce light-associated stress, perhaps through the downregulation or mobilization of LHC-antennae (Kanazawa et al. 2014; Jiang et al. 2012; Schulte et al. 2010).

Green and yellow autofluorescence signatures are representative of photo-protective and antioxidant pigments and proteins that play primary roles in photo-acclimation and stress mitigation (Figure 1.1B). Reactive oxygen species (ROS) are a well-known byproduct of photosynthesis, which can cause cellular damage in high concentrations, especially under environmental stress (Lesser 2006). Beta-carotene is an efficient reactive oxygen species (ROS) scavenger, especially in the vicinity of high concentrations of ROS (Burton 1990; Young & Britton 1993). Diadinoxanthin and diatoxanthin are the main components in the photoprotective xanthophyll cycle, dissipating excess energy through non-photosynthetic quenching (Frank et al. 1996), alongside production of antioxidants (Smerilli et al. 2016). The most abundant FbFPs (cryptochromes and riboflavin) act as key stress regulators (D'Amico-Damião et al. 2018; Yu 2010) and induce the accumulation of antioxidants (Deng et al. 2013; Taheri and Tarighi 2010; Sandoval et al. 2008). Given the high spectral overlap between proteins detected by GRN-B and YEL-B (Figure 1.1A), green and yellow fluorescence should be interpreted as redundant signatures of stress-mitigation (Figure 1.2C-D).

The protocol presented here targets key LHC pigments (RED-B, RED-R) and a combination of proteins known for their role in photo-acclimation and stress mitigation (GRN-B, YEL-B) (Figure 1.1). This provides useful insight into the cells' photosystem; however, hybridized signatures (Figure 1.1) come with limitations. For example, cells' may express different quantities of beta-carotene and diadinoxanthin or chl *a* and chl $c_2$; these are indetectable patterns as they have near indistinguishable spectral overlap within our emission filters (Figure 1.1). Individual pigment identity and abundance remains inferred. The further implementation of other filters or methods

that separate photopigments (Figure 1.1) would permit more robust interpretation of specific photopigment quantities if required. The protocol presented here is meant to be an accessible method to provide rapid insight into the single-cell state of the Symbiodiniaceae photosystem. Even with its biases and limitations, the accessibility and speed of this method makes it especially useful.

### *1.4.2 Protocol performance and optimization.*

Photopigments are fragile molecules prone to degradation in ambient conditions (Schoefs 2002); therefore, it is important to work consistently and efficiently. This includes maintaining a consistent processing environment, sample concentration, sample quantity, sample preservation, gain settings, instrument calibration, and slurry homogeny. Samples processed at room temperature were prone to rapid degradation, yielding imprecise estimates of fluorescent parameters compared to consistent autofluorescence-based physiological profiles for samples stored and processed on ice (Figure 1.2). However, autofluorescence signatures still changed dramatically after tissue removal from coral skeletons when processing was delayed, even when stored on ice. Based on our observations (Figure 1.2), I recommend that samples are processed for flow-cytometry within two hours of beginning sample preparation.

Cell concentration and flow-cytometer run-time are further factors to consider. Based on our assay (Figure 1.2), 5-fold to 10-fold dilutions of a sample with a starting concentration of ~150,000 cells/mL produced the most consistent dataset (15,000 – 30,00 cells/mL) (Figure 1.3). Informed by this assay, I have decided to locally adhere to a 10-fold dilution for all *A. pulchra* samples; however, this may differ for other species or instruments. Over-dilution led to variable means and high variances of fluorescent parameters, while under-dilution exacerbated degradation and caused cell clumping (Figure 1.3). Independent of concentration, samples began to degrade

after processing four rows (48 wells) of the 96-well plate (Figure 1.3). Therefore, I recommend loading no more than half of a 96-well plate per run with each well containing an estimated concentration of 15,000-30,000 cells/mL. None of these observed patterns are caused by settled cells, as each replicate is vortexed before being loaded into a microwell, and the flow cytometer automatically stirs each sample at a high velocity for seven seconds before data acquisition. The analyses presented here provide a roadmap for implementing and optimizing our flow-cytometry protocol, as best practice in our lab with our samples may not be best practice in your lab with your samples. I recommend investing protocol optimization time upfront. Once established, my protocol should work across a diverse set of cnidarian hosts including corals, jellyfish, and hydroids, requiring little ongoing maintenance or cost.

Under different light conditions, dinoflagellates adjust their photosystems, for example, increasing LHC pigments (peridinin, chl *a*, chl $c_2$) in dark conditions and increasing antioxidants (diadinoxanthin) in light conditions (Johnsen et al. 1994), a response successfully reflected by red and green fluorescence signatures in *Cassiopea*-associated Symbiodiniaceae using our flow cytometry protocol (Figure 1.4). Dark-acclimated individuals displayed the highest red fluorescence (peridinin, chl *a* & $c_2$ (Figure 1.1)) autofluorescence, while light-acclimated individuals displayed the lowest photopigment-associated autofluorescence (Figure 1.4A-B). Green autofluorescence displayed the inverse pattern, where dark acclimated individuals possessed the faintest green-fluorescent signatures (antioxidants (Figure 1.1)) (Figure 1.4C). I hypothesize that the mildly lower red fluorescence (LHC-associated photopigments) and elevated green fluorescence (antioxidants) in the light-acclimated group is natural acclimation, while the high red autofluorescence in conjunction with elevated green fluorescence in variable-condition individuals suggests stress (Figure 1.4). At the opposite end of the spectrum, perhaps dark-acclimated

individuals with low antioxidant and high photopigment autofluorescence could represent low stress-levels and successful acclimation (Figure 1.4).

This acclimation experiment represents an example application of our protocol for relatively simple comparisons of Symbiodiniaceae assemblages originating from different host individuals; however, the visibly small effect size is worth considering (Figure 1.4). I argue that the ability to detect extremely small, yet statistically significant effect sizes is the strength of flow cytometry. The distributional difference of means is much more statistically powerful when comparing cellular distributions that are made of thousands of observations (Symbiodiniaceae) instead of four to five (*Cassiopea*) (Figure 1.4A-C), while trends are more conspicuous but less statistically powerful when summarized to the host (Figure 1.4D-F). Despite small effect size and low statistical power, I believe the treatment effects are real given the simultaneously collected and processed samples, the use of a clonal *Cassiopea* lineage, and a mild treatment (ambient lighting). Since the goal of the method is to better understand the endosymbiotic assemblage on the level of the single cell, I find both levels of resolution informative (Symbiodiniaceae and *Cassiopea*); however resolution to single Symbiodiniaceae cells is a more accurate representation of population-level phenotypic variance. I recommend researchers wholly consider effect size given their factorial resolution. The integration of this protocol alongside other commonly used methodologies (e.g. PAM fluorometry & ITS2 metabarcoding) may help provide a more complete picture of Symbiodiniaceae acclimation and adaptation.

***1.4.3 A theoretical application.*** The ability to export fluorescent profiles for every observed Symbiodniaceae cell has theoretically high potential. For example, Symbiodiniaceae research is beginning to integrate functional diversity with genetic diversity. Perhaps our flow cytometry protocol could reveal physiological plasticity within a Symbiodiniaceae assemblage (Figure 1.5).

This may even be integrated into flow cytometric protocols that are able to partition Symbiodiniaceae functional groups based on fluorescent profiles (Apprill et al. 2007; McIlroy et al. 2014; McIlroy et al. 2020). Some of these protocols already acknowledge that they are determining functional diversity based on chlorophyll fluorescence (e.g. Apprill et al. 2007). A simple protocol modification to these studies could make these signature quantifiable and help research dive further into functional plasticity and diversity of Symbiodiniaceae.

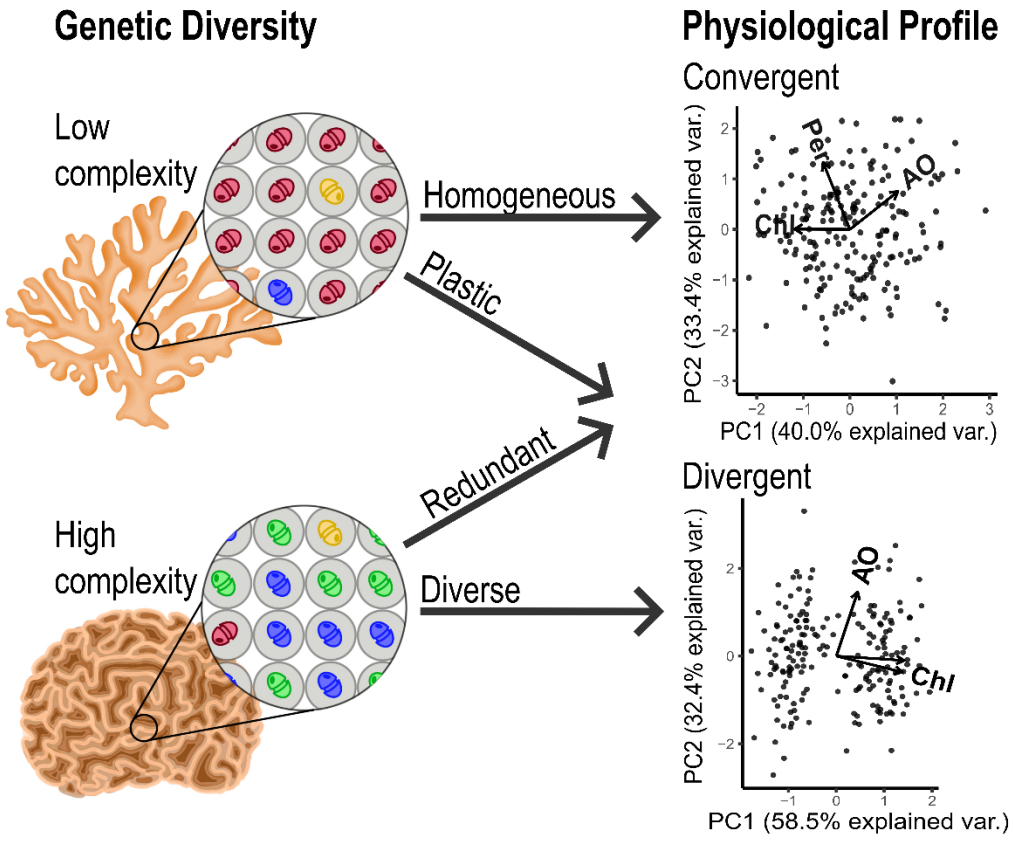


**Figure 1.5:** Phylogenetic diversity of Symbiodiniaceae assemblages in-hospite may indicate low complexity (one dominant clade) or high complexity (more than one dominant clade) communities (Davies et al. 2022). Autofluorescence profiles may be either convergent or divergent, as shown here by PCAs of consisting of chlorophylls (**Chl**), peridinin (**Per**), and antioxidants (**AO**). The combination of phylogenetic diversity and physiological profiles has the potential to allow for the classification of Symbiodiniaceae assemblage functional strategies into homogenous, plastic, redundant, or diverse categories. Simulated datasets were generated and analyzed using R.

For example, Symbiodiniaceae assemblages hosted in corals can either harbor homogeneous Symbiodiniaceae assemblages with low phylogenetic diversity (one dominant genus, species, or strain) or diverse assemblages with high phylogenetic diversity (several codominant genera, species, or strains) (Davies et al. 2022) (Figure 1.5). If a coral hosts a highly diverse Symbiodiniaceae assemblage, but only a single autofluorescence profile is detected using our flow cytometry protocol, one may assume functional redundancy of symbiont clades or mediation of symbiont physiology by the coral host (Figure 1.5). Alternatively, if a coral hosts a low diversity Symbiodiniaceae assemblage, but multiple distinct autofluorescence profiles are detected, one may assume functional plasticity of the assemblage (Figure 1.5). Unfortunately, all assemblages that I have analyzed most likely had very low genetic complexity (*Acropora pulchra*: Anthony et al. 2022c; *Cassiopea:* Thornhill et al. 2006), which could explain the observed convergent physiological profiles. Despite this, I hope the promising results from the example application data presented here (Figure 1.4), as well as other early research using this protocol (Chapter 2), suggests that the integration of our protocol could provide helpful insights into the Cnidaria-associated Symbiodiniaceae assemblage.

**1.5 Acknowledgements**

I would like to thank Colin Lock and Bastian Bentlage for their contribution to this work. I would like to thank Rebecca Salas for allowing me to use her jellyfish and for running the upside-down jellyfish acclimation experiment. I would also like to thank MacKenzie Heagy for illustrating the coral-dinoflagellate assemblages shown in Figure 1.5.

## 1.6 References


Anthony CJ, Lock CC, Bentlage B (2022a) High-throughput physiological profiling of endosymbiotic dinoflagellates (Symbiodiniaceae) using flow cytometry. Protocols.io. https://dx.doi.org/10.17504/protocols.io.dm6gpjr2jgzp/v1

Anthony CJ, Heagy MH, Bentlage B (2022b) Phenotypic plasticity in *Cassiopea ornata* (Cnidaria: Scyphozoa: Rhizostomeae) suggests environmentally driven morphology. Zoomorphology 141:115-131. https://doi.org/10.1007/s00435-022-00558-5

Anthony CJ, Lock C, Taylor BM, Bentlage B (2022c) Photosystem regulation in coral-associated dinoflagellates (Symbiodiniaceae) is the primary mode for seasonal acclimation. bioRxiv 2022.12.24.520888. https://doi.org/10.1101/2022.12.24.520888

Berg JT, David CM, Gabriel MM, Bentlage B (2021) Fluorescence signatures of persistent photosystem damage in the staghorn coral *Acropora* cf. *pulchra* (Anthozoa: Scleractinia) during bleaching and recovery. Mar Biol Res 16(8-9):643-655. https://doi.org/10.1080/17451000.2021.1875245

Bricaud A, Claustre H, Ras J Oubelkheir K (2004) Natural variability of phytoplanktonic absorption in oceanic waters: Influence of the size structure of algal populations. J Geophysical Research Oceans 109(C11). https://doi.org/10.1029/2004JC002419.

Bujak Ł, Piatkowski D, Mackowski S, Wörmkeb S, Jungb C, Bräuchleb C, Agarwalc A, Kotovc NA, Schulted T, Hofmannd E, Brotosudarmoe THP, Scheere H, Govorovf AO, Hilleret RG (2009) Plasmon enhancement of fluorescence in single light-harvesting complexes from *Amphidinium carterae.* Acta Phys Pol 116:S22-S25. https://doi.org/10.12693/APhysPolA.116.S-22

Burton GW (1990) Antioxidant properties of carotenoids. J Nutr 119:109–111.

Davies S, Gamache MH, Howe-Kerr LI, Kriefall NG, Baker AC, Banaszak AT, Bay LK, Bellantuono AJ, Bhattacharya DC, Debashish C, et al (2022) Building consensus around the assessment and interpretation of Symbiodiniaceae diversity. https://doi.org/10.20944/preprints202206.0284.v1

D'Amico-Damião V, Carvalho RF (2018) Cryptochrome-related abiotic stress responses in plants. Front Plant Sci 19. https://doi.org/10.3389/fpls.2018.01897

Deng B, Jin X, Yang Y, Lin Z, Zhang Y (2014) The regulatory role of riboflavin in the drought tolerance of tobacco plants depends on ROS production. Plant Growth Regul 72:269–277. https://doi.org/10.1007/s10725-013-9858-8

Dubelaar GB, Jonker RR (2000) Flow cytometry as a tool for the study of phytoplankton. Scientia Marina. 64(2):135-136. https://doi.org/10.3989/scimar.2000.64n2135

Fernandes de Barros Marangoni L, Ferrier-Pagès C, Rottier C Bianchini A, Grover R (2020) Unravelling the different causes of nitrate and ammonium effects on coral bleaching. Sci Rep 10:11975. https://doi.org/10.1038/s41598-020-68916-0

Figueroa RI, Howe-Kerr LI, Correa AMS (2021) Direct evidence of sex and a hypothesis about meiosis in Symbiodiniaceae. Sci Rep 11:18838. https://doi.org/10.1038/s41598-021-98148-9

Frank, Cua A, Chynwat V, Young A, Gosztola D, Wasielewski MR (1996) The lifetimes and energies of the first excited singlet states of diadinoxanthin and diatoxanthin: the role of these molecules in excess energy dissipation in algae. Biochim Biophys Acta Bioenerg 1277:243-252.

Fujise L, Nitshke MR, Frommlet JC, Serodio J, Woodcock S, Ralph PJ, Suggett DJ (2018) Cell cycle dynamics of cultured coral endosymbiotic microalgae (*Symbiodinium*) across different types (species) under alternate light and temperature conditions. J Eukaryot Microbiol. 65(4):505-517. https://doi.org/10.1111/jeu.12497

Fujita S, Iseki M, Yoshikawa S, Makino Y, Watanabe M, Motomura T, Kawai H, Murakami A (2005) Identification and characterization of a fluorescent flagellar protein from the brown alga *Scytosiphon lomentaria* (Scytosiphonales, Pheophyceae): a flavoprotein homologous to Old Yellow enzyme. Eur J Phycol 40:159-167. https://doi.org/10.1080/09670260500063193

Hennige SJ, Suggett DJ, Warner ME, McDougall KE, Smith DJ (2009) Photobiology of *Symbiodinium* revisited: Bio-physical and bio-optical signatures. Coral Reefs 28:179-195. https://doi.org/10.1007/s00338-008-0444-x

Hiller RG, Wrench PM, Gooley AP, Shoebridge G, Breton J (1993) The major intrinsic light-harvesting protein of Amphidinium: Characterization and relation to other light-harvesting proteins. Photochem Photobiol 57(1):125–131. https://doi.org/10.1111/j.1751-1097.1993.tb02267.x

Hoegh-Guldberg O (1999) Climate change, coral bleaching and the future of the world's coral reefs. Mar Freshw Res 50:839-866.

Jeffrey SW (1989) Chlorophyll c pigments and their distribution in the chromophyte algae. In: Green JC, Leadbeater BSC, Diver WL. (eds) The Chromophyte Algae: Problems and Perspective. Systematics Association. Clarendon, Oxford. 38:13–36.

Jiang J, Zhang H, Kang Y, Bina D, Lo CS, Blakeship RE (2012) Characterization of the peridinin–chlorophyll *a*-protein complex in the dinoflagellate *Symbiodinium* Biochim Biophys Acta Bioenerg 1817(7):983-989. https://doi.org/10.1016/j.bbabio.2012.03.027

Johnsen G, Nelson NB, Jovine RVM, Prézelin BB (1994) Chromoprotein- and pigment-dependent modeling of spectral light absorption in two dinoflagellates, Prorocentrum minimum and *Heterocapsa pygmaea*. Mar Ecol Prog Ser 114(3):245-258.

Kagatani K, Nagao R, Shen JR, Yamano Y, Takaichi S, Akimoto S (2022) Excitation relaxation dynamics of carotenoids constituting the diadinoxanthin cycle. Photosynth Res 154:13-19. https://doi.org/10.1007/s11120-022-00944-5

Kanazawa A, Blanchard GJ, Szabó M, Ralph PJ, Kramer DM (2014) The site of regulation of light capture in *Symbiodinium*: Does the peridinin–chlorophyll *a*–protein detach to regulate light capture? Biochim Biophys Acta Bioenerg 1837(8):1227-1234. https://doi.org/10.1016/j.bbabio.2014.03.019

Kassambara A (2020) ggpubr: 'ggplot2' Based Publication Ready Plots. R package version 0.4.0. https://CRAN.R-project.org/package=ggpubr

Kawalska D, Krajnik B, Olejnik M, Twardowska M, Czechowski N, Hofmann E, Mackowski S. (2013) Metal-enhanced fluorescence of chlorophylls in light-harvesting complexes coupled to silver nanowires. Sci World J 2013:670412. https://doi.org/10.1155/2013/670412

Kleinegris DMM, van ES MA, Janssen M, Brandenburg WA, Wijffels RH (2010) Carotenoid fluorescence in *Dunaliella salina*. J Appl Phycol 22:645-649. https://doi.org/10.1007/s10811-010-9505-y

Koyama Y, Hashimoto H (1983) Spectroscopic studies of carotenoids in photosynthetic systems. In: Young AJ, Britton G. (eds) Carotenoids in Photosynthesis. Springer, Dordrecht. https://doi.org/10.1007/978-94-011-2124-8_9

Koziol B, Markowicz M, Kruk J, Plytycz B (2007) Riboflavin as a source of autofluorescence in *Eisenia fetida* coelomocytes. Photochem. Photobiol. 82(2):570-3. https://doi.org/10.1562/2005-11-23-RA-738

Krediet CJ, DeNofrio JC, Caruso C, Burriesci MS, Cella K, Pringle JR (2015) Rapid, Precise, and Accurate Counts of *Symbiodinium* Cells Using the Guava Flow Cytometer, and a Comparison to Other Methods. PLOS ONE. 10(8):e0135725. https://doi.org/10.1371/journal.pone.0135725

Lee CS, Yeo YSW, Sin TM (2012) Bleaching response of *Symbiodinium* (zooxanthellae): Determination by flow cytometry. Cytom Part A 81A(10):888-895. https://doi.org/10.1002/cyto.a.22111

Lesser MP (1996) Elevated temperatures and ultraviolet radiation cause oxidative stress and inhibit photosynthesis in symbiotic dinoflagellates. Limnol Oceanogr 41(2):271-283. https://doi.org/10.4319/lo.1996.41.2.0271

Lesser MP (2006) Oxidative stress in marine environments: Biochemistry and physiological ecology. Annu Rev Physiol 2006; 68:253-278. https://doi.org/10.1146/annurev.physiol.68.040104.110001

Maruyama S, Shoguchi E, Satoh N, Minagawa J (2015) Diversification of the light-harvesting complex gene family via intra- and intergenic duplications in the coral symbiotic alga *Symbiodinium*. PLOS ONE. 10:e0119406.

McKinnon, K. M (2018) Flow cytometry: An overview. Curr Protoc Immunol 120:5.1.1–5.1.11. https://doi.org/10.1002/cpim.40

Mukherjee A, Walker J, Weyant KB, Schroeder CM (2013) Characterization of Flavin-Based Fluorescent Proteins: An Emerging Class of Fluorescent Reporters. PLOS ONE 8(5):e64753. https://doi.org/10.1371/journal.pone.0064753

Mullaney PF, Van Dilla MA, Coulter JR, Dean PN (1969) Cell sizing: a light scattering photometer for rapid volume determination. Rev Sci Instrum 40: 1029-1032.

Muscatine L, Porter JW (1977) Reef corals: Mutualistic symbioses adapted to nutrient-poor environments. BioScience 27:454-460.

Muscatine L, Falkowski PG, Porter JW, Dubinsky Z (1984) Fate of photosynthetic fixed carbon in light- and shade-adapted colonies of the symbiotic coral *Stylophora pistillata*. Proc R Soc Lond B. 222:181–202.

Niedzwiedzki DM, Jiang Jing CSL, Blankenship RE (2014) Spectroscopic properties of the Chlorophyll *a*–Chlorophyll $c_2$–Peridinin-Protein-Complex (acpPC) from the coral symbiotic dinoflagellate *Symbiodinium*. Photosynth Res 120:125-139. https://doi.org/10.1007/s11120-013-9794-5

Ogle DH, JC Doll, Wheeler P. Dinno A (2022) FSA: Fisheries Stock Analysis. R package version 0.9.3. https://github.com/fishR-Core-Team/FSA

Polívka T, Hiller RG, Frank HA (2007) Spectroscopy of the peridinin–chlorophyll-*a* protein: insight into light-harvesting strategy of marine algae. Arch Biochem Biophys 458:111–120. https://doi.org/10.1016/j.abb.2006.10.006

R Core Team (2021) R: A language and environment for statistical computing. R Foundation for Statistical Computing, Vienna, Austria. https://www.R-project.org/

RStudio Team (2020) RStudio: Integrated Development for R. RStudio, PBC, Boston, MA. http://www.rstudio.com/

Sandoval FJ, Zhang Y, Roje S (2008) Flavin nucleotide metabolism in plants. J Biol Chem 283(45):30890-30900. https://doi.org/10.1074/jbc.M803416200

Schoefs B (2002) Chlorophyll and carotenoid analysis in food products: Properties of the pigments and methods of analysis. Trends Food Sci Technol 13(11):361-371. https://doi.org/10.1016/S0924-2244(02)00182-6

Shapiro HM (2003) Practical Flow Cytometry. 4th Edition. NJ: Wiley-Liss.

Siddiqui PJA, Carpenter EJ (1992) Ultrastructure and immunolocalization of phycobiliproteins and ribulose 1,4-bisphosphate carboxylase/oxygenase in the marine cyanobacterium *Trichodesmium thiebautii*. J Phycol 28:320–327.

Smerilli A, Orefice I, Corato F, Olea AG, Ruban AV, Brunet C (2016) Photoprotective and antioxidant responses to light spectrum and intensity variations in the coastal diatom *Skeletonema marinoi*. Environ Microbiol 19(2):611-627. https://doi.org/10.1111/1462-2920.13545

Steen M (1980) Further developments of a microscope-based flow cytometer: Light scatter detection and excitation intensity compensation. Cytometry 1:26-31.

Subramaniam A, Carpenter EJ (1999) Bio-optical properties of the marine cyanobacteria *Trichodesmium* spp. I. Absorption and photosynthetic spectra. Limnol Oceanogr 44: 608–617.

Suprasi KM, Kumar M, Segecova A, McCauley JI, Herdean A, Padula MP, O'Meara T, Ralph PJ (2021) Characterisation and bioactivity analysis of peridinin-chlorophyll *a*-protein (PCP) isolated from *Symbiodinium tridacnidorum* CS-73. J. Mar Sci Eng 9(12):1387. https://doi.org/10.3390/jmse9121387

Suwa R, Hirose M, Hidaka M (2008) Seasonal fluctuation in zooxanthellar genotype composition and photophysiology in the corals *Pavona divaricata* and *P. decussata.* Mar Ecol Prog Ser 381:129-137.

Taheri P, Tarighi S (2010) Riboflavin induces resistance in rice against *Rhizoctonia solani* via jasmonate-mediated priming of phenylpropanoid pathway. J Plant Physiol. 167:201–208. https://10.1016/j.jplph.2009.08.003

Tzur A, Moore JK, Jorgensen P, Shapiro HM, Kirschner MW (2011) Optimizing optical flow cytometry for cell volume-based sorting and analysis. PLOS ONE 6(1):e16053. https://doi.org/10.1371/journal.pone.0016053

Venn AA, Wilson MA, Trapido-Rosenthal HG, Keely BJ, Douglas AE (2006) The impact of coral bleaching on the pigment profile of the symbiotic alga, *Symbiodinium*. Plant Cell Environ. 29:2133-2142. https://doi.org/10.1111/j.1365-3040.2006.001587.x

Warner ME, Fitt WK, Schmidt GW (1996) The effects of elevated temperature on the photosynthetic efficiency of zooxanthellae *in hospite* from four different species of reef coral: a novel approach. Plant Cell Environ. 19(3):291-299. https://doi.org/10.1111/j.1365-3040.1996.tb00251.x

Watson JV (1991) Introduction to Flow Cytometry. Cambridge: Cambridge University Press.

Wickham H (2016) ggplot2: Elegant Graphics for Data Analysis. Springer New York https://doi.org/10.1007/978-0-387-98141-3

Yacobi YZ (2012) From Tswett to identified flying objects: A concise history of chlorophyll *a* use for quantification of phytoplankton. Isr J Plant Sci 60(1). https://doi.org/10.1560/IJPS.60.1-2.243

Yoon HS, Havkett JD, Bhattacharya D (2002) A single origin of the peridinin- and fucoxanthin-containing plastids in dinoflagellates through tertiary endosymbiosis. Proc Nat Acad Sci 99(18):11724-11729.

Young A. Britton G (1993) Carotenoids in Photosynthesis. Chapman and Hall, London, England.

Yu X, Liu H, Klejnot J, Lin C (2010) The Cryptochrome Blue Light Receptors. Arabidopsis Book 8:e0135. https://doi.org/10.1199/tab.0135

Zapata M, Edvardsen B, Rodriguez F, Maestro MA, Garrido JL (2001) Chlorophyll $c_2$ monogalactosyldiacylglyceride ester (chl $c_2$- MGDG). A novel marker pigment for *Chrysochromulina* species (Haptophyta). Mar Ecol Prog Ser 219:85-98. https://www.doi.org/10.3354/meps219085

## Chapter 2

## Spatio-Temporal Acclimation and Adaptation of the Symbiodiniaceae Assemblages Associated with Guam's Dominant Staghorn Coral *Acropora pulchra*

### 2.0 Summary

Coral-associated dinoflagellates (Symbiodiniaceae) play a primary role in coral acclimation and adaptation. Symbiont shuffling, cell density regulation, and phenotypic plasticity have all been proposed as mechanisms to adjust to environmental change. However, few studies have been able to partition which of the three strategies is responsible for observed phenotypic variance. Therefore, I quantified the biodiversity, cell density, and phenotypic variance of *Acropora pulchra*-associated Symbiodiniaceae assemblages across five sites and two time points. Samples were collected from 20 GPS-tagged colonies across five reef flats representing all known *A. pulchra*-containing environments around Guam during the onset of seasonal warming and the highest sea water temperatures of the year. Symbiodiniaceae assemblages displayed site and season-specific phenotypic variance, while biodiversity and cell densities in host tissues remained seasonally stable. Symbiodiniaceae biodiversity was relatively low diversity yet displayed distinct geographic organization. Based on these patterns, I identify phenotypic plasticity as the source of phenotypic variation and is likely the primary mode of acclimation to mild environmental change, while changes in biodiversity are a form of long-term assemblage adaptation after acute selective events or chronic environmental stressors.

## 2.1 Introduction

In corals, each coral colony supports its own unique assemblage of organisms, with each symbiotic combination having the capability to create a functionally distinct coral (Gates and Ainsworth 2011). Symbiodiniaceae are dinoflagellates known for their endosymbiotic relationship with many marine invertebrates including Cnidaria, Mollusca, Porifera, Platyhelminthes, Foraminifera, and Ciliata (LaJeunesse et al. 2018). The ecological success of reef-building corals (Scleractinia) has been attributed to this endosymbiotic relationship between corals and their dinoflagellate endosymbionts (Symbiodiniaceae) given its independent evolution multiple times through coral history (Gault et al. 2021). Corals are highly dependent on these micro-algal endosymbionts for nutrient acquisition and effective calcification (Falkowski et al. 1984; Muscatine et al. 1984; Baker et al. 2013; Roth 2014; Matthews et al. 2017; Ezzat et al. 2017), but environmental stress can lead to a functional breakdown of this photo-endosymbiotic relationship, leading to the expulsion of Symbiodiniaceae from the host (coral bleaching) and often death (Brown 1997). Climate change has increased the frequency and severity of coral bleaching globally (Hughes et al. 2017). The survival of corals in stressful environments can be linked to differences in the ecological tolerances of Symbiodiniaceae (Parkinson et al. 2015; Thornhill et al. 2014).

An ecosystem's functional capabilities are driven by the functional characteristics of its inhabitants (Hooper et al. 2005); therefore, a better understanding of an ecosystem only comes after identifying an ecosystem's biodiversity and its dynamics. The recent taxonomic redescription of the Family Symbiodiniaceae illustrated more divergent lineages and more distinct morphological variation and genomic divergence between clades than previously thought (LaJeunesse et al. 2018). Over 400 distinct assemblage phylotypes have been described, each with

different photosynthetic, nutrient exchange, and thermoresilience capabilities (Berkelmans and van Oppen 2006; LaJeunesse et al. 2009; Swain et al. 2020). The combination of these phylotypes build diverse symbiotic communities, which produce functionally distinct coral holobionts (Baker 2003; Stat et al. 2008; Wall et al. 2020), and in turn, differentially resilient coral reefs. Some lineages, such as *Durusdinium*, offer high thermotolerance in exchange for decreased carbon and nitrogen fixation in their hosts (Keshavmurthy et al. 2014; Silverstein et al., 2017). However, species-level functional differences can be equally distinct as genus-level functional differences (Mansour et al. 2018). Within genus functional diversity was well illustrated in a tank experiment with *Acropora millepora* colonies from of the Great Barrier Reef, which showed the highest resilience when dominated by *Cladocopium* C3k, while the least resilient colonies were inhabited mostly by *Cladocopium* C1232 (Howe-Kerr et al. 2020).

In the short term, Symbiodiniaceae communities seem largely controlled by the host and in the long term, the environment seems more likely to shift symbiont communities (Baker et al. 2018; Camp et al. 2019; Howe-Kerr et al. 2020). If the environment shifts, and endosymbionts are not functionally advantageous, successful acclimation may be caused by shifts in endosymbiont community composition, known as symbiont shuffling (Buddemeier and Fautin 1993; Baker 2003; Jones et al. 2008). For example, *Durusdinium* is more common in stressful environments (Fabricius et al. 2004; LaJeunesse et al. 2010) or after acute stress events (Baker et al. 2004; Berkelmans and van Oppen 2006). However, endosymbiotic Symbiodiniaceae community composition can also be remarkably stable (Rouzé et al. 2019) indicating a high level of host-symbiont specificity and in turn implying high acclimation potential through phenotypic plasticity (Goulet 2006). Species of Symbiodiniaceae have been experimentally shown to have varying rates of plasticity to environmental change (Mansour et al. 2018); therefore, I predict that the

acclimation and adaptation strategy of a coral-associated Symbiodiniaceae assemblage is dependent on the inhabitants of the assemblage itself in conjunction with the environmental change it regularly experiences.

In addition to Symbiodiniaceae assemblage adaptation through shifts and shuffling of Symbiodiniaceae, assemblages have many proposed methods of acclimation through phenotypic plasticity. Generally, Symbiodiniaceae acclimation revolves around modifying the efficiency and productivity of their photosystem, as it is the most direct way to regulate ATP and NADPH formation, and in turn, the quantity of harmful and beneficial metabolic byproducts (Oakley et al. 2014). While photosystem acclimation is typically tied to the modification of photosystem photochemistry (Warner et al. 2002; Ulstrup et al. 2008; Nitshke et al. 2018), the physical reorganization and regulation of photopigments, as well as adjustments to cell morphology, can also mitigate stress and promote successful acclimation to different light conditions and may be a better representation of long term (months vs days) system regulation (Johnsen et al. 1994; Sawall et al. 2014; Xiang et al. 2015; Oliveira et al. 2022). Photoacclimation in situ is well studied along light attenuation gradients including depth (Warner et al. 2002; Iglesias-Prieto et al. 2004; Frade et al. 2008; Lesser et al. 2010; Cooper et al. 2010) and turbidity (Hennige et al. 2008; Suggett et al. 2012). Changes in physiology during seasonal acclimation is also reasonably well described (Ulstrup et al. 2008; Sawall et al. 2014; Nitschke et al. 2018) given the functional variance of Symbiodiniaceae phylotypes and their ability to differentially regulate their photosystems and demonstrating variable sensitive to high light acclimation after thermal exposure (Robison and Warner 2006). However, most of this research uses PAM fluorometry to quantify the overall photosynthetic efficiency of the system (Warner et al. 1996, Warner et al. 2002; Ralph and Gademann 2005; Szabó et al. 2014) and not the underlying phenotype (physiology, morphology,

behavior) of individuals within the quantified Symbiodiniaceae assemblage. While informative, this resolution is not ideal for in-situ (within the field) or in-hospite (within the host) research aiming to better understand acclimation of single cells because the reading can be affected by microalgal density and a host morphology (e.g. skeletal morphology) (Wangpraseurt et al. 2019). This makes it difficult to partition whether changes in photophysiology, as detected by PAM, are caused by changes in community composition, endosymbiotic cell densities, single-cell phenotypic plasticity, or other factors. Alternatively, flow cytometry can rapidly quantify phenotypic profiles on a per cell basis, mitigating the scalar biases associated with PAM fluorometry (discussed in Chapter 1).

Symbiont shuffling, cell density regulation, and phenotypic plasticity have all been proposed as mechanisms to adjust to environmental change (Jones and Yellowlees 1997; Baker 2001; Baker 2003; Baker 2004; Goulet 2006). Despite the plethora of knowledge on Symbiodiniaceae photophysiology, much of our knowledge has not closed the gap in resolving how changes in physiology are explained by adaptation (shifts or shuffles in symbiont) versus acclimation (physiology of existing community). For example, Symbiodiniaceae cells experience no decline in photopigment abundance during coral bleaching (Venn et al. 2006). This could mean two things: (1) physiological acclimation of Symbiodiniaceae is separate from coral bleaching suggesting decoupled acclimation strategies or (2) Symbiodiniaceae have low physiological plasticity suggesting any major change in physiological readings reflect changes in the underlying Symbiodiniaceae community. Revealing whether shifts in physiology are a byproduct of acclimation through phenotypic plasticity or adaptation through changes in Symbiodiniaceae diversity or abundance would provide insight into the resilience, adaptation strategies, and natural

history of coral-associated Symbiodiniaceae and help us inform the scale and focus of future resilience-based research.

In this study, I aimed to characterize the *A. pulchra*-associated Symbiodiniaceae assemblage at a community (biodiversity), population (cell density), and individual level (morphology and physiology) simultaneously under natural environmental conditions. The genus Acropora Oken 1815 is the most diverse and abundant of modern corals making it a popular subject for present research (Wallace 1999). *Acropora pulchra* (Brook, 1891) is a fast-growing staghorn coral, which contributes substantially to reef structure providing refuge to a highly diverse assemblage of fish and invertebrates. With increased biodiversity comes increased functional capacity of an ecosystem (Hooper et al., 2005); therefore, the structurally complex and fast-growing nature of staghorn corals should directly support resilient reefs in a changing climate. However, staghorn corals are heavily impacted by anthropogenic pressures due to their fragile skeletal structure and susceptibility to tidal exposure, high temperatures, and disease (Raymundo et al. 2017). In Guam, *A. pulchra* is the most abundant staghorn coral; however, with just two consecutive years of anomalously warm sea surface temperature events and extreme tides caused the population to decline by over 300,000 square meters (~33% of their estimated distribution) (Raymundo et al. 2017; Raymundo et al. 2019). Stress events select for resilient populations, meaning that it is possible the most resilient Symbiodiniaceae assemblage is found in surviving *A. pulchra* populations. The repeated sampling of Guam's dominant staghorn corals, which have survived many recent acute stress events, provide succinct and novel insight on Symbiodiniaceae assemblage acclimation and adaptation under both long term and short-term environmental change.

## 2.2 Materials and Methods

***2.2.1 Colony selection and host identification.*** To identify the dynamics of Symbiodiniaceae assemblages under natural seasonal fluctuation on an island-wide scale, four thickets of *A. pulchra* from five reef flats (20 thickets total) were GPS-tagged around the island of Guam (Micronesia): Urunao (N 13.63672° E 144.84527°), West Agaña (N 13.47993° E 144.74278°), Luminao (N 13.46584° E 144.64496°), Togcha (N 13.36865° E 144.774967°), and Cocos Lagoon (N 13.24596° E 144.68475°) (Figure 2.1).

No coral bleaching was seen at any site for 2021; however these sites represent a range of unique bleaching histories, geographical distribution, coral biodiversity, and environmental conditions (cf. Raymundo et al., 2017; Raymundo et al., 2019). Urunao (North) was a pristine, shallow site with dense thickets of *A. pulchra* evenly distributed from the algal-dominated reef crest to the beach. The sampled colonies formed small clusters of 0.25-1 $m^2$ colonies. The high skeletal density of coral colonies is due to the constant high wave energy and shallow reef. The surrounding coral community had a relatively high species richness (16) with a live coral to hard substrate to soft substrate ratio of 1:1:1. West Agaña (Northwest) appeared to have a large community of *A. pulchra* exposed to moderate water movement on the outside and extremely low water movement on the inside. However, surveys revealed a relatively low live coral cover to substrate ratio (1:4) and diversity (9) when compared to other sites indicating a highly impacted reef system. Luminao (West) had a small, scattered population of reasonably large thickets nested within an extensive *Porites*-dominated reef with a gentle, steady current driven by strong wave energy on a distant algal ridge. Like Urunao, Luminao had a relatively high coral diversity, but conversely to Urunao and other sites, the Luminao reef surrounding tagged *A. pulchra* colonies was dominated by live coral over substrate. Cocos Lagoon (South) has a few small thickets of *A.*

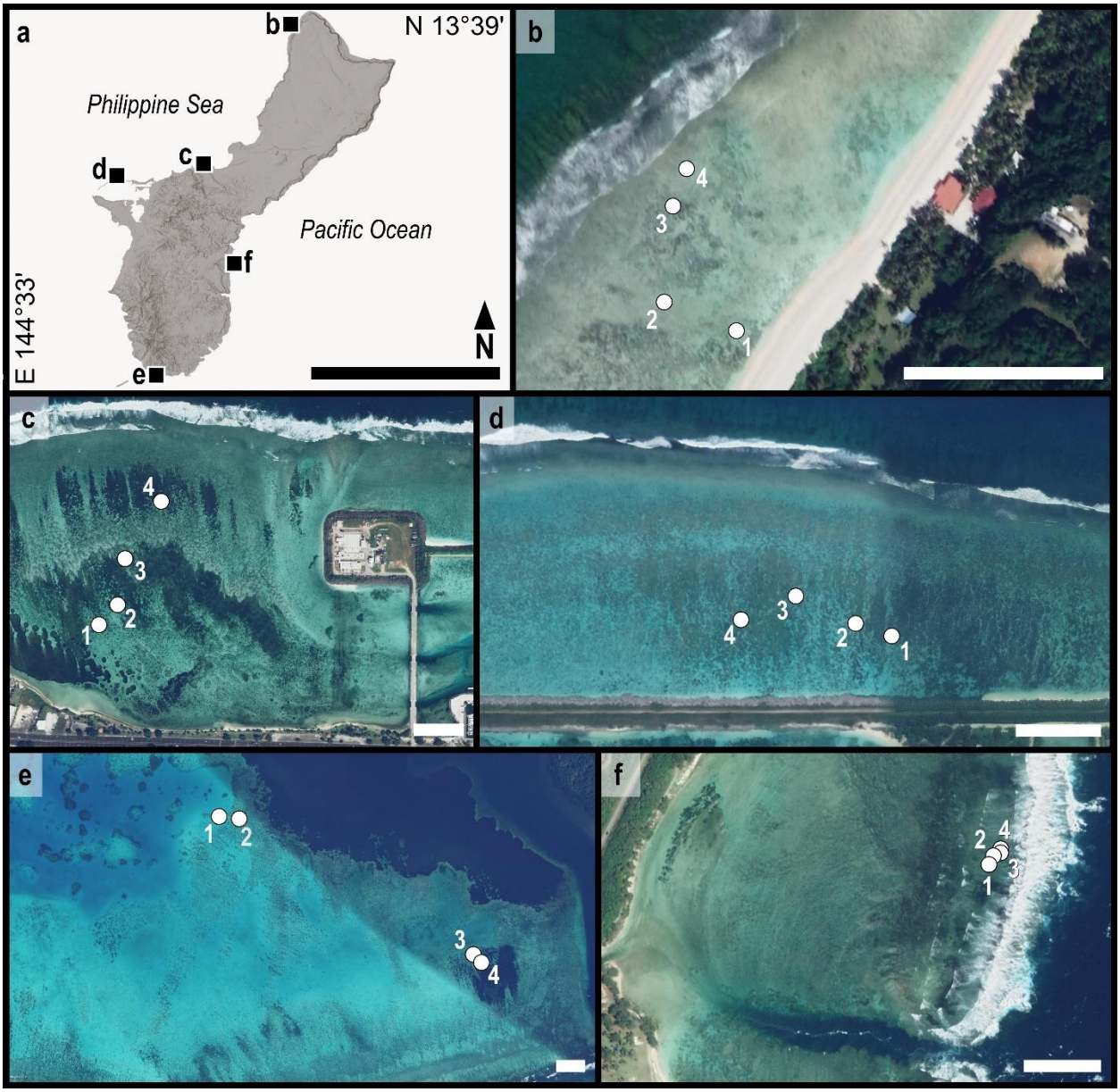


**Figure 2.1. A**) Sampling sites in Guam (scale: 20 km) with each square indicating the location of a reef flat sampled for this study: **B**) Urunao (North), **C**) West Agaña (Northwest), **D**) Luminao (West), **E**) Cocos Lagoon (South), and **F**) Togcha (East). **b**-**f**) Within each site, four thickets (**1**-**4**) of *A. pulchra* were georeferenced for repeated sampling. Images provided by Google Earth Pro v7.3.4.8248. (scale: 100 m)

*pulchra* growing within the lagoon surrounded by sand and the three dominant poritiids (massive *Porites*, *Porites cylindrica*, and *Porites rus)*. The other two colonies were within extremely low diversity (5), extensive, shallow water (~1 m) *Acropora aspera* thickets near the edge of the lagoon. Colonies in Cocos Lagoon were notably the least healthy of the entire island with active

*Terpios* sponge infections on most colonies. The only known east-coast population of *A. pulchra*, Togcha (East), is limited to a single population in the high wave energy zone near the reef crest (Figure 2.1). All colonies had an extremely high skeletal density and the surrounding reef had by far the highest coral diversity. From this point forward sites will primarily be referred to, not by their site name, but by the cardinal direction they best represent ('North' = Urunao, 'Northwest' = West Agaña, 'West' = Luminao, 'South' = Cocos Lagoon, and 'East' = Togcha).

*Acropora pulchra* colonies were identified and physically selected using a combination of past population genetics research (Rios 2020) and systematic knowledge on corallite morphology (e.g. half-crescent corallite shape). After tagging colonies, mitochondrial DNA sequences for the mitochondrial control region (COX-3) were generated to support our assumption of consistent host identification. Genomic DNA was extracted from each sample fragment using the DNeasy® PowerSoil Pro Kit®. Sequences were amplified by polymerase chain reaction (PCR) with the forward rns_FP1 and reverse cox3_RP1 primers for mitochondrial COX-3 sequences (van Oppen et al. 2001). Each PCR reaction volume was 25 µL consisting of 1 µL of DNA (20 ng/µl), 0.75 µl of 10 µM forward primer, 0.75 µl of 10 µM reverse primer, 0.75 µl of 2.5 mM dNTP, 16 µl water, 5 µl buffer (10x), and 0.75 µl Taq (TaKaRa Taq™ DNA Polymerase 1U). The PCR profile was 94°C for 180 s, 32 cycles of 94°C for 20 sec, 56°C for 30 sec, 72°C for 1.5 min, and a final extension at 72°C for 5 min. PCR products with single strong bands visualized with gel electrophoresis were cleaned with the GeneJET PCR purification kit. Samples were sequenced in both directions and consensus sequences were generated in Geneious Prime v2021.1.1 (Biomatters, Auckland, NZ). Sequences were aligned against publicly available sequences on NCBI and with locally generated unpublished sequences with MAFFT v7.475 (Katoh and Standley 2013) using the G-INS-i strategy. Poorly aligned regions were filtered using gblocks v0.91b

(Castresana 2000) as implemented in Seaview v5.0.4 (Guoy et al. 2020), allowing for smaller final blocks, gap positions, and less strict flanking positions. An approximately-maximum-likelihood phylogenetic tree was inferred using FastTree v2.1.11 (Price et al. 2010). Additionally, a maximum parsimony haplotype network (P = 0.95) with haplotypes v1.1.2 (Aktas, 2020) R v4.1.2 (R Core Team 2021) in RStudio v1.3.1073 (RStudio Team 2020). Phylogenetic tree and haplotype network were visualized and edited with FigTree v1.4.4 (Rambaut 2018) and Inkscape v1.1 (https://inkscape.org/).

***2.2.2 Environmental characterization.*** To characterize island-wide seasonal environmental changes, average sea surface temperature (SST) (NOAA Coral Reef Watch 2019) and precipitation (Menne et al. 2012a; Menne et al. 2012b) data were obtained for Guam in 2021. Bleaching risk was assessed using NOAA's virtual field station for Guam (Liu et al. 2018). Additionally, historical wave height, period, and cardinal direction were downloaded for 2012-2022 from wave buoys at Ritidian Point (N Guam) and Ipan (SE Guam), provided by the Pacific Islands Ocean Observing System (PacIOOS; www.pacioos.org).

***2.2.3 Tissue sampling.*** From the island-representative sites, three tissue samples per thicket were collected with sterile stony coral cutters from at least three centimeters below the axial growth tip. This was repeated for all 20 GPS-tagged colonies within two seasonally relevant time periods: 30 April - 18 May (1) and 28 July - 15 August 2021. All samples were immediately flash-frozen in liquid nitrogen on site, then stored at -80 °C until processing. These samples were subsequently used to quantify Symbiodiniaceae biodiversity, cell density, and phenotype, which were processed simultaneously to keep all dependent variables paired to the exact source fragment.

***2.2.4 Symbiodiniaceae ITS2 biodiversity.*** Genomic DNA was extracted using a Qiagen DNeasy PowerSoil Pro Kit (Qiagen, Hilden, Germany) on a Qiacube connect liquid handling system. The ITS2 region was amplified via PCR with SYM_VAR_5.8S2 and SYM_VAR_REV primers (Hume et al. 2018) using 3 µL of DNA (10 ng/µl), 3 µl of 10 µM primer, 2.4 µl of 2.5 mM dNTP, 18.6 µl water, 3 µl buffer (10x), and 0.15 µl Taq (TaKaRa Taq™ DNA Polymerase 1U). The PCR profile was 26 cycles of 95°C for 40 s, 59°C for 120 s, 72°C for 60 s, and a final extension at 72°C for 420 s. ITS2 amplicons were multiplexed and sequenced on a NovaSeq 6000 (250bp Paired-end; Illumina, San Diego, CA, USA). Paired-end reads were initially analyzed using the SymPortal pipeline with default parameters (Hume et al. 2019) to identify Symbiodiniaceae lineages and assign ITS2 type profiles.

***2.2.5 Symbiodiniaceae cell density.*** Coral tissue was airbrushed from the skeleton with filtered seawater (FSW) and homogenized using a vortexer and syringe needle-shearing, and then subsequently processed using the protocol described in Chapter 1.

Absolute cell counts were obtained by multiplying cytometry-generated cell concentrations by each sample's dilution factor and tissue homogenate volume to determine total cell count for each coral tissue fragment. Cell density per $cm^2$ (Equation 1) was obtained by the normalization of cytometry-derived cell counts to the source fragment's skeletal surface area. To determine skeletal surface area, I created a three-dimensional model for each coral fragment built from point clouds with 0.010 mm point spacing generated by a jewelry scanner (D3D-s, Vyshneve, Ukraine). Prior to scanning, coral fragments were coated with SKD-S2 Aerosol (Magnaflux, Glenview, IL) to reduce skeletal light refraction. Point clouds of each fragment were imported into MeshLab v2020.04 (Cignoni et al. 2008) to generate a surface mesh by Poisson surface reconstruction.

Portions of the fragment that were not covered in tissue prior to airbrushing were removed from the reconstructed surface prior to surface area estimation.

$$(1) \qquad Cell\ Density = \frac{Cell\ Count \cdot Dilution \cdot Total\ Homogenate\ Volume}{Sample\ Surface\ Area}$$

***2.2.6 Symbiodiniaceae phenotyping.*** While in Chapter 1, I describe multiple signatures that could be used to quantify an entire physiological profile for Symbiodiniaceae, in this study I only use readings from the RED-B laser to simplify the narrative and only present the most conservative results. From this point forward red fluorescence RFI values will be considered to represent relative photopigment abundance (Lesser 1996; Lee et al. 2012; Cooper et al. 2014; Anthony et al. 2022).

In the previous chapter, fluorescent side scatter and forward scatter were used to inform cell lysing and swelling during different sample preparation methods, respectively. In this chapter, I use fluorescent side scatter and forward scatter to complete our cytometry-derived phenotypic profile. When cells are hit with a laser, a certain amount of laser hits the cell, and is scattered in alternative directions. This fluorescent scatter is detected by sensors in the flow cytometer and can be used as a metric to represent cell roughness (Mullaney et al. 1969; Steen 1980; Watson 1991; Shapiro 2003). Similarly, fluorescent forward scatter refers to any fluorescence detected by a sensor behind the cell, on the opposite end of the machine from the excitation laser; this reading is used to quantify cell size (Mullaney et al. 1969; Steen 1980; Watson 1991; Shapiro 2003; Tzur et al. 2011).

***2.2.7 Statistical Analysis.*** Symbiodiniaceae community structure was compared across sites (North, Northwest, West, South, East) and seasons (May, August). Modelled after Eckert et al. (2020), relative ITS2 sequence abundances and type profiles were normalized and visualized after

metabarcoding data was preprocessed with the SymPortal pipeline (Hume et al. 2019). Multivariate homogeneity of dispersion (PERMDISP), pairwise permutation tests, and a permutational multivariate analysis of variance (PERMANOVA) were conducted on normalized ITS2 type profiles using Vegan v2.5-7 (Oksanen et al. 2020) and pairwise Adonis v0.4 (Martinez Arbizu 2017) packages. PERMDISP used Bray-Curtis similarity and permutation tests used Bray-Curtis dissimilarity. Permutation tests were run with 9999 replicates.

Cytometric data (cell density, red fluorescence, forward scatter, and side scatter) violated the assumption of parametric tests of a normal data distribution, as determined by Shapiro-Wilk tests ($p < 0.001$); therefore all statistical tests were non-parametric and did not assume normality.

To understand the relationship between cell density, red fluorescence, side scatter, and forward scatter, simple non-parametric Spearman correlations were calculated for two groupings of paired dependent variables: (1) cell density, red fluorescence, side scatter, and forward scatter averaged to the fragment-level triplicate sample replicate and (2) red fluorescence, side scatter, and forward scatter without any value summarization, given that flow cytometry automatically produces paired RFI data for each cell detected. Calculations were completed using rstatix v0.7.1 (Kassambara 2022).

To evaluate factorial contributions to Symbiodiniaceae phenotype and cell density, repeated measures, univariate analyses of variance (RM-ANOVA) were performed to evaluate the response of cell density, red fluorescence, forward scatter, and side scatter using the MANOVA.RM package v0.5.3 (Friedrich et al. 2022). This test neither assumes multivariate normality nor covariance matrix specificity, making it robust to repeated measure designs with factorial nesting (Friedrich et al. 2019). Main and interaction effects were resampled with 1000

non-parametric bootstrap replicates and corrected p-values were calculated for type statistics (Friedrich et al. 2019; Friedrich et al. 2022). Prior to any statistical tests, 1000 observations for each group were randomly sampled for each cytometry replicate (often from a sample size of > 100,000 per cell measurements) to reduce the computational requirements of statistical tests and decrease the likelihood of overinterpretation.

In addition to the repeated measures tests, data from the 40 sampling events (five sites, two timepoints, and 20 colonies) was evaluated with non-parametric Kruskal-Wallis tests ($X^2$) and pairwise Dunn's tests, as integrated in the FSA package v0.9.3 (Ogle et al. 2022). Statistical outputs were then converted to statistical groups based on distributional similarity and difference using _rcompanion v2.4.21 (Mangiafico 2023). Each sample distribution was assigned to a statistical group (a-s) based on the results of pairwise Dunn's tests, which better visualized data structure and similarity, improving the interpretation of previously calculated repeated measures tests. A distribution would be in the same group as another distribution if they were not statistically different (e.g. $p > 0.001$), while distributions would appear in different groups if they were statistically different (e.g. $p < 0.001$). Cell density data distributions were grouped with a standard threshold of $p = 0.05$, while phenotypic measurements were grouped with a threshold of $p = 0.001$ to avoid the overinterpretation of effect sizes made stronger by a high sample size (n=1000).

To test whether underlying phenotypic variation was caused by plasticity or biodiversity, ITS2 type profiles identified by metabarcoding were mapped to their fragment's associated phenotypic profile generated by flow cytometry. Phenotypic measurements for the North (the only site with heterogenous Symbiodiniaceae biodiversity) were compared using a combination of Kruskal-Wallis and Dunn's tests; with the same process described in the previous paragraph.

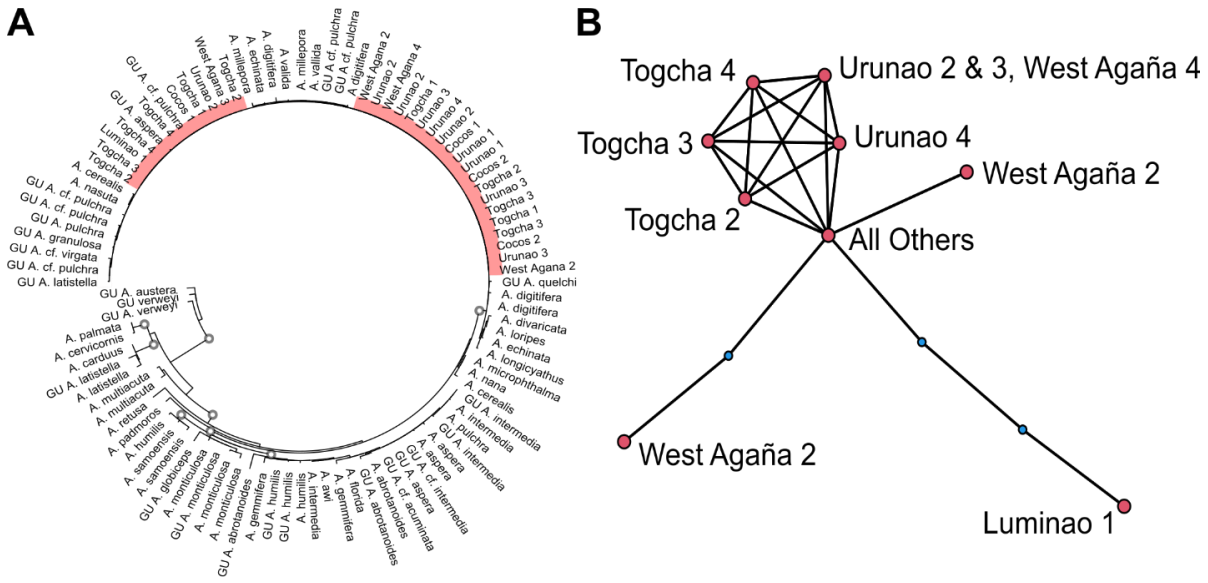


**Figure 2.2**. **A**) Approximate-Maximum-Likelihood Tree made using the COX-3 region from representatives of *Acropora*. The shaded region highlights sequences from tagged colonies and their site of origin (Figure 2.1). White circles indicate highly supported nodes on the phylogenetic hypothesis backbone (FastTree support value: >0.9). **B**) Haplotype network of COX3 sequences from tagged colonies indicating two major haplotypes with nine maximum haplotypes indicated by large pink circles. Each line indicates a single nucleotide difference.

All data curation and statistical analyses were completed with R v4.1.2 (R Core Team 2021) in RStudio v1.3.1073 (RStudio Team 2020) unless otherwise indicated. Figures were generated and modified with primarily with a combination of ggplot2 v3.3.5 (Wickham 2016), ggpubr v0.4.0 (Kassambara 2020), and InkScape v1.1 (https://inkscape.org).

## 2.3 Results

***2.3.1 Host Identification.*** The phylogenetic tree and haplotypes network suggest extremely high genetic similarity, with sequences typically only differing by a single nucleotide (Figure 2.2). I recognize that coral population genetics and systematics often requires extremely high genomic sampling and that the COX-3 region is not the ideal gene region to understand host genetic diversity, as indicated by the extremely low-resolution phylogeny (Figure 2.2A). However, given

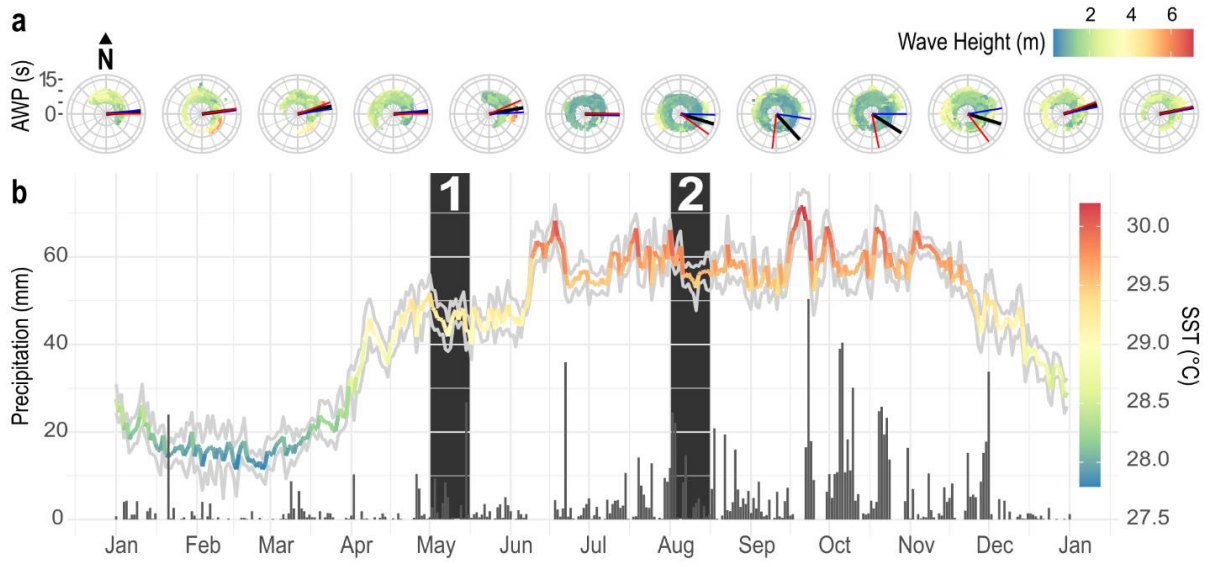


**Figure 2.3 A**) Spectral polar plots of aggregated historical wave data from Ritidian (**red lines**) and Ipan (**blue lines**) wave buoys. Monthly mean wave direction (**black lines**) indicated prevailing swells from the East, the windward side of Guam. Waves were higher with shorter periods from January to April, the season that sees strong westerly trade winds. (Provided by PacIOOS (www.pacioos.org)). **B**) Average sea surface temperature (SST) (**spectral line**) (NOAA Coral Reef Watch, 2019), and precipitation (**grey bars**) (Menne et al., 2012a; Menne et al., 2012b) for 2021 showed distinct seasonal patterns. The first set of samples was collected in the first two weeks of May (**1**) during the transitional warming period, while the second set of samples was collected in the first two weeks of August (**2**) during the hot, rainy season.

the high clonality of *A. pulchra*, as identified by previous population genetics research from Guam (Rios 2020), I can reasonably assume that most colonies are *A. pulchra*. If any corals were a misidentification, I would suspect either West Agana 2 or Luminao 1 as indicated by their two and three nucleotide differences (Figure 2.2B). After analyzing the rest of the data, these outlier colonies did not represent any unique biodiversity, cell density, or phenotypic variance.

***2.3.2 Environment.*** Guam has distinct windward (East) and leeward sides (West), hence the relevance of labeling sites as cardinal directions in the previous section. According to the publicly available environmental data provided by PacIOOS (www.pacioos.org), wave energy on Guam was highest from December to March with waves, on average, coming from the East year-round (Figure 2.3A), the island's windward side. In 2021, Guam did not enter a coral bleaching warning (NOAA Coral Reef Watch 2019), presumably due to La Niña, supporting our observations that no

bleaching was observed or reported. Therefore, 2021 represents a year characterized by mild seasonal fluctuations. The water temperature increased steadily from March to June, remaining stable during the following four months. Precipitation followed a similar trend (Figure 2.3B). May represented a seasonal transition with warming waters and decreasing wave energy; August was characterized by environmental stasis with high water temperatures and low wave energy (Figure 2.3B).

***2.3.3 Symbiodiniaceae biodiversity.*** Symbiodiniaceae communities of *A. pulchra* were largely dominated by *Cladocopium* C40 (Figure 2.3a). Total biodiversity and beta-diversity dispersion was determined by site and not by time (Table 1; Figure 2.4). ITS2 type profiles showed Symbiodiniaceae community overlap along Guam's western coast, while southern and eastern IT2 type profiles were distinct.

**Table 1.** Outputs of PERMANOVA and PERMDISP to determine factorial contributions for ITS2-type diversity and ITS2 beta-diversity, respectively.

| | COMMUNITY | | | |
|---|---|---|---|---|
| | ITS2-type | | Beta-diversity | |
| | F | p | F | p |
| Time | 0.437 | 0.761 | 0.014 | 0.906 |
| Site | 88.793 | 0.001 | 11.725 | <0.001 |

Pairwise permutation tests revealed the North as an outlier, as it was the only site with a *Durusdinium* ITS2 type profile. A pairwise permutation test of the North across seasons indicated that communities were not statistically differentiated between sampling time points ($F = 0.5426815$, $R^2 = 0.4945$, $p = 0.4945$); however, plot-specific data suggested *Cladocopium*-*Durusdinium* partitioning from nearshore to farshore colonies, with *Durusdinium* being more common nearshore (Figure 2.7).

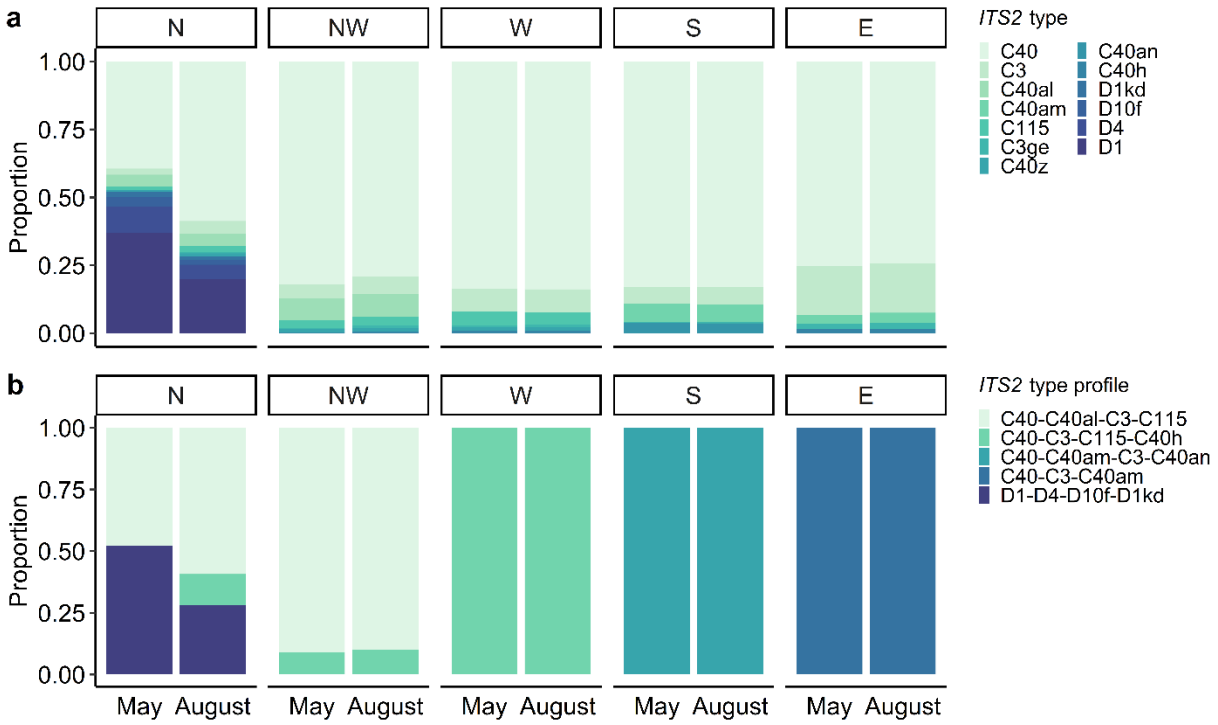


**Figure 2.4:** ITS2 type diversity (**A**) and ITS2 type profiles (**B**) from spatio-temporal sampling across five sites (North, Northwest, West, South, and East) and two timepoints (May and August).

***2.3.5 Symbiodiniaceae cell density.*** Cell density only varied with time (t = 20.81, p = 0.042) (Table 2), which was primarily driven by changes in cell density at the southern and eastern sites (Figure 2.6). Pairwise Dunn's tests did not reveal any obvious factorial structuring (Figure 2.6A). Cell density was not correlated to any phenotypic metric (ρ = 0.096, p = 0.299; ρ = 0.021, p = 0.822; ρ = 0.03, p = 0.742).

| | POPULATION | |
|---|---|---|
| | Cell Density | |
| | t | p |
| **Time** | 20.81 | 0.042 |
| **Site** | 0.917 | 0.44 |
| **Time:Site** | 2.99 | 0.159 |
| **Site:Plot** | 0.758 | 0.516 |
| **Time:Site:Plot** | 0.711 | 0.528 |

**Table 2.** RM-ANOVA testing the factorial contribution to variation in cell density.

***2.3.6 Symbiodiniaceae phenotypic variation.*** Symbiodiniaceae phenotypic metrics were heavily influenced by time ($t = 2165.49$, $p < 0.001$), site ($t = 4859.68$, $p < 0.001$), and site within time ($t = 18.661$, $p < 0.001$) (Table 3). Red fluorescence (photopigment abundance) was most influenced by site ($t = 291.668$, $p < 0.001$); although it was also well influenced by time ($t = 1056.04$; $p = 0.002$) (Table 3). Generally, red fluorescence declined from May to August, aside from a few plot-specific scenarios, while the site showed a more complex, case-specific partitioning of statistical groups (Figure 2.5B). Side scatter (cell roughness) demonstrated a similar data structure of case-specific partitioning but was especially influenced by site measurements within time ($t = 86.503$, $p < 0.001$) and did not visually indicate any macro pattern (Figure 2.5C). Forward scatter (cell size) was the cleanest data structure, heavily structuring with Site within Time ($t = 322.342$, $p < 0.001$), and experiencing comparatively little within site data variation (Table 3; Figure 2.5D). Generally, colonies decreased red fluorescence and forward scatter with temporal sampling; however, East colonies demonstrated a reciprocal pattern from the rest of the island with smaller cells in May and larger cells in August.

Time seemed to be especially influential of cell phenotype with low phenotypic variance in May and a wide phenotypic variance in August (Figure 2.6A-E). The East site maintained a wide phenotypic variance through both temporal sampling points (Figure 2.6E). All phenotypic variables were correlated to each other ($p < 0.001$) (Figure 2.6F).

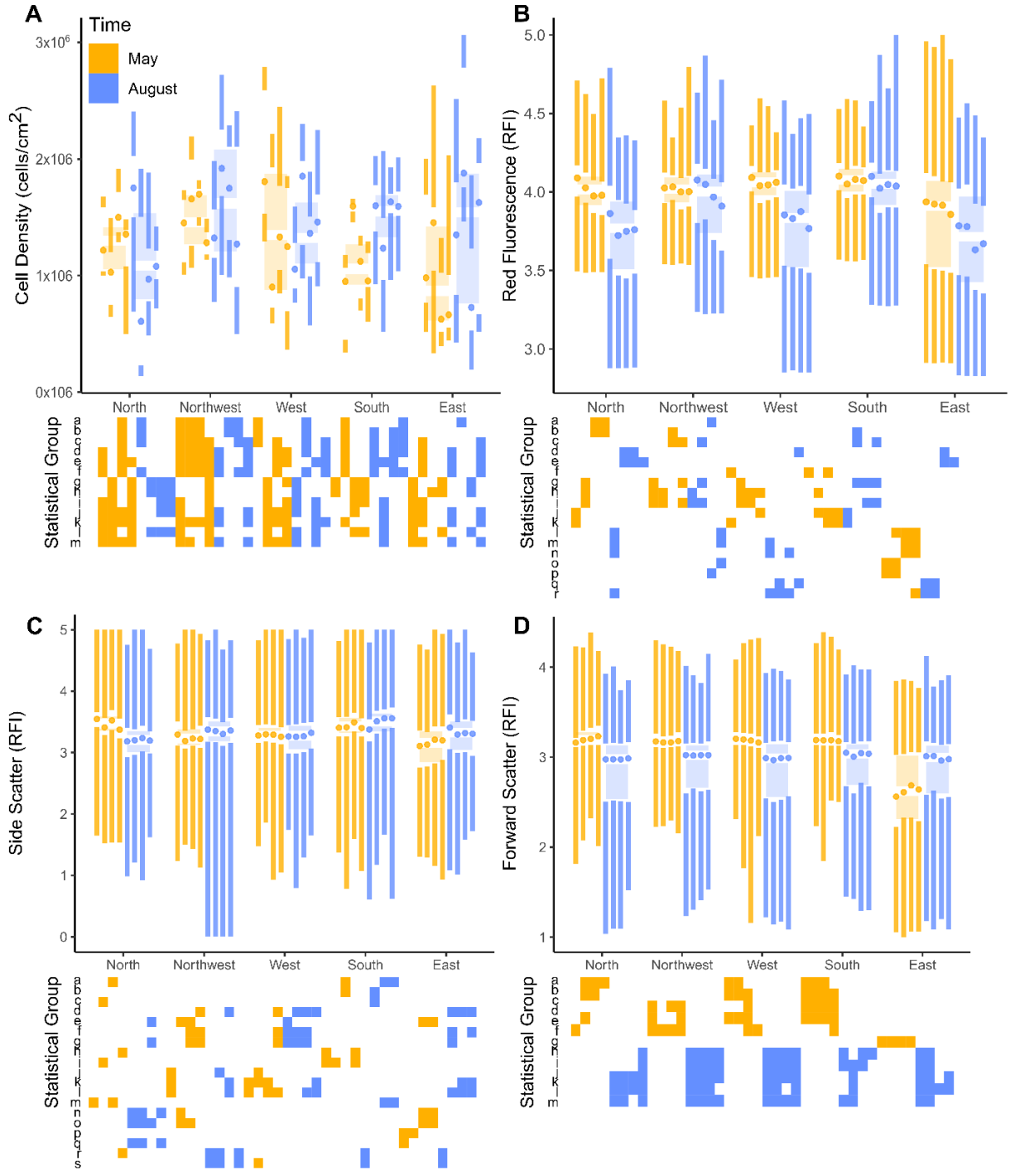


**Figure 2.5**: Cell density and phenotype variance visualized as boxplots (Site * Season) and Tuft's boxplots (Plot * Site * Season). Colors indicate temporal sampling. Statistical groupings (squares) supported by pairwise Dunn's tests (**A:** $p < 0.05$; **B-D:** $p<0.001$) reveal data structure hidden by most visualizations and broader statistics. **A)** Cell density shows almost no statistical structure. **B-C)** Red fluorescence (photopigment abundance) and side scatter (cell roughness) show statistically supported, case-specific factorial contributions. **D)** Forward scatter shows high temporally structured statistical groupings.

**Table 3.** RM-MANOVA and three RM-ANOVAs testing the factorial contribution to variation in red fluorescence, side scatter, and forward scatter.

| | INDIVIDUAL | | | | | | | |
|---|---|---|---|---|---|---|---|---|
| | RED, FSC, SSC | | RED | | SSC | | FSC | |
| | t | p | t | p | t | p | t | p |
| **Time** | 2165.49 | <0.001 | 1056.04 | 0.002 | 33.978 | 0.02 | 5071.41 | 0.001 |
| **Site** | 4589.68 | <0.001 | 208.903 | <0.001 | 44.468 | 0.002 | 414.256 | <0.001 |
| **Time:Site** | 18.661 | <0.001 | 48.343 | 0.003 | 86.503 | <0.001 | 322.342 | <0.001 |
| **Site:Plot** | 162.621 | 0.116 | 2.643 | 0.172 | 2.863 | 0.17 | 2.073 | 0.230 |
| **Time:Site:Plot** | 93.414 | 0.242 | 0.808 | 0.489 | 2.434 | 0.195 | 1.567 | 0.313 |

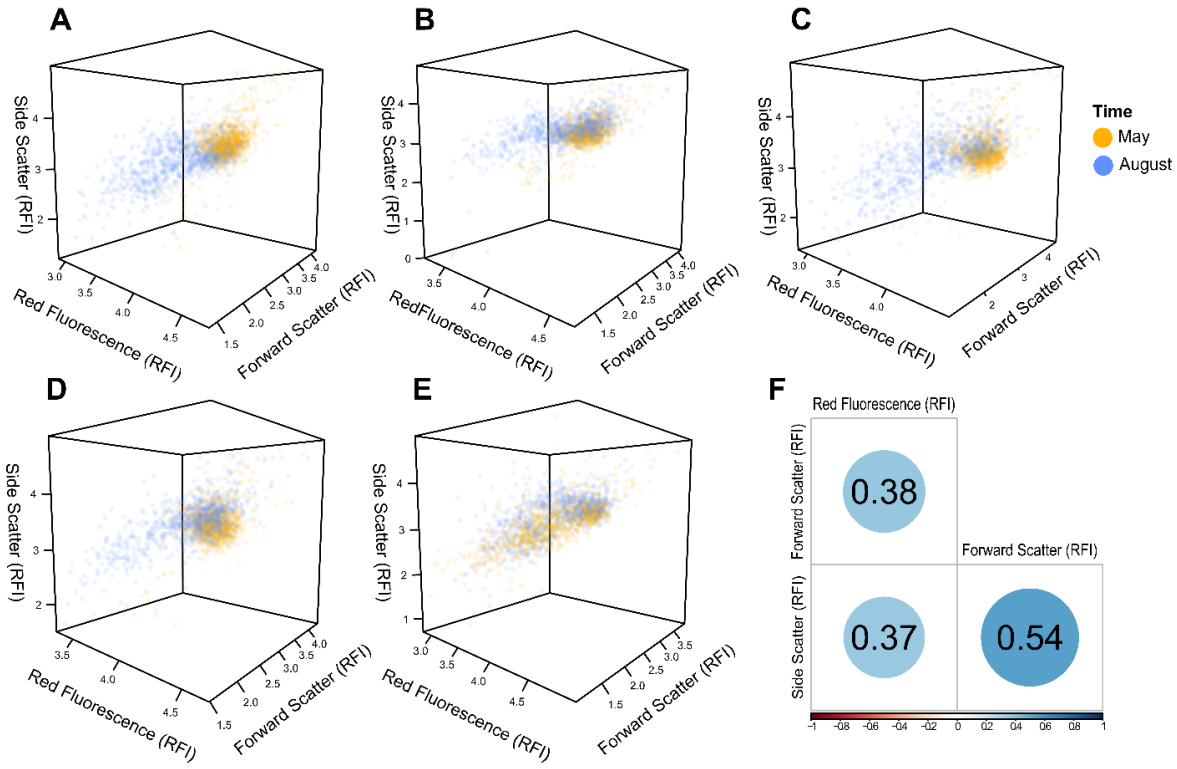


**Figure 2.6. A-E**) Three-dimensional dot plots visualizing phenotypic profiles for North (**A**), Northwest (**B**), West (**C**), South (**D**), and East (**E**) Symbiodiniaceae assemblages across repeated temporal sampling (May & August). **F**) Pairwise spearman correlation rho values ($p < 0.001$) for red fluorescence, forward scatter, and side scatter.

***2.3.7 Biodiversity-phenotype association.*** As discussed in previous sections, only one of the five sites indicated co-dominance of ITS2 type profiles within a reef (Figure 2.3). Within this site, type profiles progressed from nearshore *Durusdinium*-dominated colonies to farshore *Cladocopium*-dominated colonies (Figure 2.7); therefore, plots were compared to evaluate whether ITS2-type profiles were associated with phenotypic variance. Independent from plot, type profiles did not differ in cell density ($X^2 = 5.7604$, df = 2, p = 0.05612); despite a visually lower cell density mean in *Durusdinium*-dominated (D1-D4-D10f) colonies (Figure 2.7A). Plot-specific measurements illustrated a general increase in cell density as corals approached the wave break, although accompanied by high variance. For fluorescence-based measurements, the geography structure of ITS2 type profiles made partitioning type-related differences difficult. Two *Durusdinium*-dominated and two *Cladocopium*-dominated colonies co-occured at Plot 2 and Plot 3 providing some direct phenotypic comparisons. For colonies within Plot 2, type profile indicates possible phenotypic differences; however, co-occuring colonies of the same type profile also demonstrated some statistical difference (e.g. *Cladocopium*-dominated colonies in Plot 3) (Figure 2.7).

## 2.4 Discussion

***2.4.1 Geographic structuring of Symbiodiniaceae diversity.*** I found that *A. pulchra*-associated Symbiodiniaceae communities were geographically structured and temporally stable (Figure 2.3). Long-term monitoring of endosymbiotic communities has described high stability and colony-level specificity (Rouze et al. 2019); however, this high fidelity in *A. pulchra* is surprising. In *Acropora*, Symbiodiniaceae are acquired from the environment (Baird et al. 2009), suggesting a more flexible and diverse assemblage compared to other coral genera (e.g. Qin et al. 2019; Rouzé et al. 2017). In contrast, coral colonies sampled by us were almost exclusively dominated by *Cladocopium* C40, with only one site containing *Durusdinium* D1 (Figure 2.3). C40 and D1

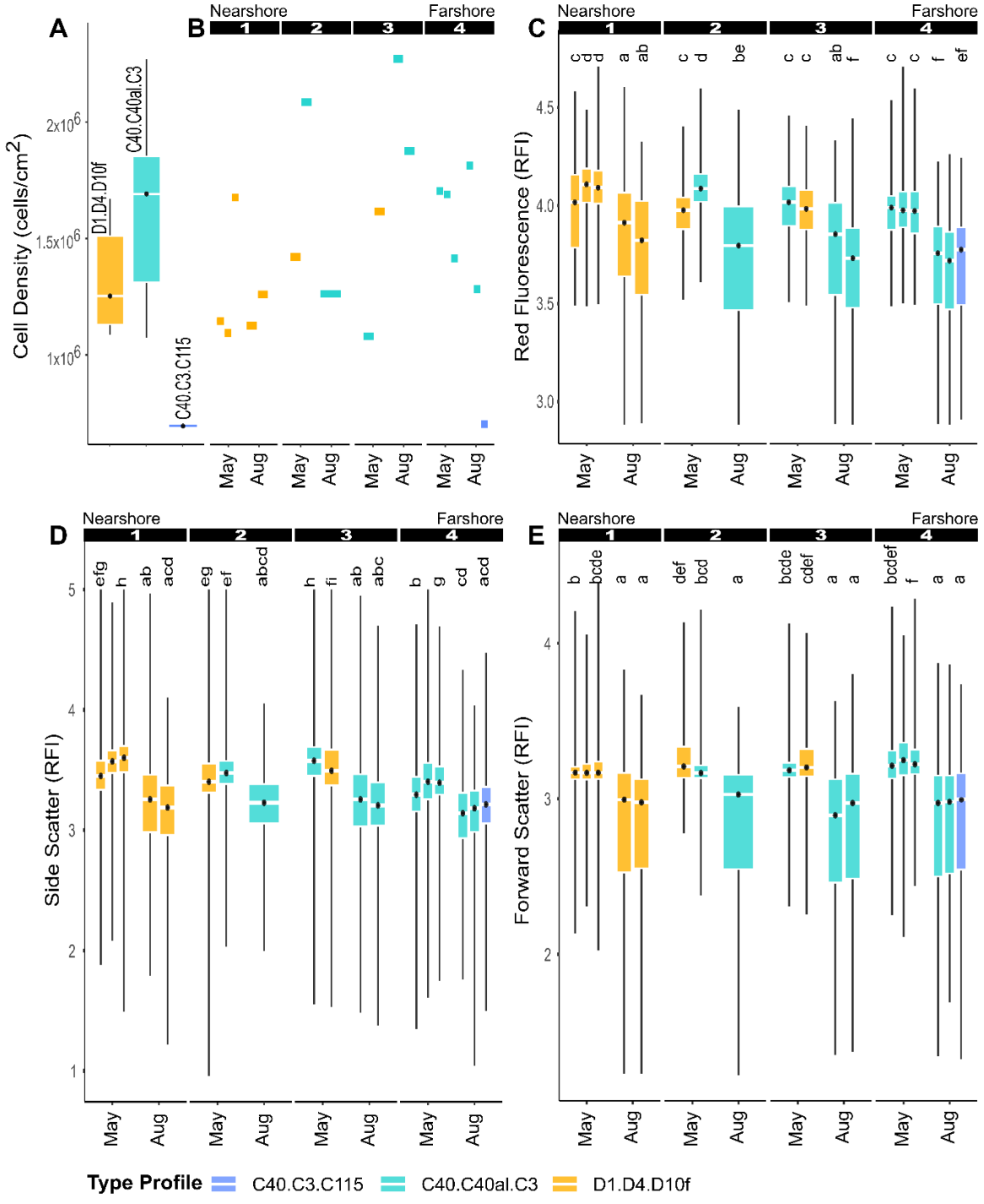


**Figure 2.7:** Cell density (**A-B**) and phenotypic measurements (**C-E**) were mapped to samples with successfully identified ITS2 type profiles. Sampled plots incrementally stepped across the reef flat from nearshore to farshore (1-4) (c.f. Figure 2.1). Separate box plots indicate different colonies sampled within their respective plots (Figure 2.1). **C-E**) Letters above each boxplot indicate statistically supported groupings ($p < 0.001$). Different letters indicate statistical dissimilarity, while the same letter between two boxplots indicate statistical similarity.

represent important lineages associated with reduced coral bleaching rates and increased coral survival following stress (Jones et al. 2008; Mieog et al. 2009; Rouzé et al. 2017; Qin et al. 2019).

The co-occurrence of D1-dominated and C40-dominated ITS2 type profiles within the North site (a narrow, shallow reef flat) suggests similar resilience to acute stress events, while the nearshore to farshore partitioning could indicate differential resilience to long term chronic stressors or environmental conditions. Perhaps *Durisdinium* was selected for its tolerance to slightly warmer waters (Stat et al. 2008; Keshavmurthy et al. 2014; Silverstein et al. 2017), assumed by its nearshore position. This supports the hypothesis that the environment seems more likely to shift symbiont communities in the long term (Baker et al. 2018; Camp et al. 2019; Howe-Kerr et al. 2020). If the environment shifts, and Symbiodiniaceae are not functionally advantageous, successful acclimation may be caused by shifts in community composition, known as symbiont shuffling (Buddemeier and Fautin 1993; Baker 2003; Jones et al. 2008; Zhu et al. 2022). The dominance of *Cladocopium* C40 and *Durusdinium* D1 in *A. pulchra* on Guam's dynamic reef flats may be the result of selection, perhaps a result of recent environmentally driven mass coral mortality events (Raymundo et al. 2017; Raymundo et al. 2019). Perhaps the original acquisition of C40 and D1 lineages occurred during coral larval settlement, increasing the likelihood of their survival during stress events (Suzuki et al. 2013). Alternatively, the present *A. pulchra* community could be composed of genets that successfully switched symbiont communities in response to extreme environmental stress (Buddemeier and Fautin 1993).

***2.4.2 Stochastic variation in cell densities.*** No trends were apparent in the cell density data (Figure 2.5A) suggesting that no factors included in this study were good predictors of cell density. This was not an anticipated result as corals visually changed color between temporal sampling (Figure 2.8), and other studies looking at seasonal acclimation of Symbiodiniaceae found a decline in cell

density during the hottest part of the year (Fitt et al. 2000; Warner et al. 2002; Ulstrup et al. 2008). The lack of a factorial correlation presented in this study is unlikely to be a methodological resolution issue as I used the highest resolution cell counting methodology in the field: high-throughput flow cytometry (Krediet et al. 2015) combined with high-resolution, three-dimensional scanning (Reichert et al. 2016). The result presented here may have been caused by a relatively mild temporally related temperature increase, a possible byproduct of 2021's La Niña event.

***2.4.3 Spatio-temporal phenotypic variation.*** All phenotypic variation was specific to plot, site, and time (Table 3; Figure 2.5). Geographically correlated ITS2 biodiversity and stochastic cell densities indicates that Symbiodiniaceae phenotypic plasticity is the primary mode of acclimation to local environmental conditions and mild environmental change. All phenotypic metrics demonstrated some level of positive correlation with each other (Figure 2.6), a reasonably well described relationship (e.g. Cooper et al. 2014); and no phenotypic metrics were correlated to cell density. Therefore, phenotypic variation was not associated with variation in cell density.

Red fluorescence decreased from May to August in all colonies (Figure 2.5B) indicating an overall reduction of photopigments; the generally expected result based on other literature (Porter et al. 1984; Brown et al. 1999; Mass et al. 2007), however, an increase in photopigments to seasonal warming has also been reported (Sawall et al. 2014). Cell roughness, measured by fluorescent side scatter, illustrated a very similar data structure (Figure 2.6C). While poorly studied, cell roughness may be another method for cells to control their light intake, and in turn their productivity. Xiang et al. (2015) found that in lower light conditions, Symbiodiniaceae reduced the amount of surface adhesion proteins produced, and gained a smoother, less complex surface mortality. Perhaps rougher cells scatter a greater amount of light, thus limiting the amount of light available to intercellular photosynthetic plastids while a smoother cell could scatter less

light, allowing more access for light to reach the light harvesting structures. Unfortunately, the lack of clear spatio-temporal structuring in our side scatter data makes it difficult to resolve any relationship between side scatter and environment.

In contrast to photopigment fluorescence and cell roughness, cell size had an extremely clean temporal data structure, primarily demonstrating larger cells in May and smaller cells in August (Figure 2.5D). Perhaps this pattern is a broad, seasonal pattern related to the rate of cell division. Under heat stress, Symbiodiniaceae proliferation decreases and cells swell (Fujise et al. 2018), which would lead to us detecting larger cells; this is not what we saw as cells were smaller during the warm season in all except one site. While we do not see signs of heat stress, warmer temperatures do slow Symbiodiniaceae cell growth and decrease photosystem productivity (Karim et al. 2015). This is more representative of the pattern observed here; however, one site complicates this interpretation.

East colonies demonstrated a different phenotypic profile than the other sites with a much higher phenotypic variance in May than other sites (Figure 2.6). In May, windward colonies (East) displayed a reciprocal pattern in cell size compared to other sites, starting with smaller cells in May and converging on the cell sizes more characteristic of the rest of the island in August. Despite this, the temporal change in red fluorescence and side scatter of East corals was not much different than other sites (Figure 2.5B-C). The only known surviving *A. pulchra* on the windward side of Guam occurs in a limited area near the East site's algal ridge (Figure 2.1F). From December to May, the windward side experienced a high frequency of large swells (Figure 2.2A), which likely improved gas exchange (Finelli et al. 2006) and increased the availability of inorganic carbon, conditions that would increase the photosynthetic rates of Symbiodiniaceae (Dennison & Barnes 1988), and in turn the abundance of metabolic byproducts and cellular population. Interestingly,

these windward coral colonies displayed a distinctive green hue in May, presumably caused by green fluorescent protein (GFP), which was absent in August and not observed at other sites (Figure 2.8). If the coral host does not regulate its Symbiodiniaceae endosymbionts, either through ROS scavenging or cell density regulation, the relationship can switch from symbiotic to parasitic (Cunning and Baker 2013; Morris et al. 2019). Coral-host GFP expression has been linked to stress mitigation through shading of photosymbionts (Lyndby et al. 2016) and antioxidant activity (Palmer et al. 2009). Perhaps the visible expression of GFP (Figure 2.8), coinciding with high phenotypic variation (Figure 2.6), smaller cells (Figure 2.5D), and a normal cell density (Figure 2.5A), was a form of host regulation to avoid a breakdown of symbiosis. In June, warming waters, decreased water flow, and increased rainfall may have made host-mediated symbiont regulation unnecessary amidst La Niña, which could explain the island-wide convergence of phenotypic variance (Figure 2.5; 2.6). This is simply a hypothesis and requires validation, but I can at least conclude that colonies in the east site were under different environmental pressures, leading to distinct phenotypic patterns and acclimation strategies.

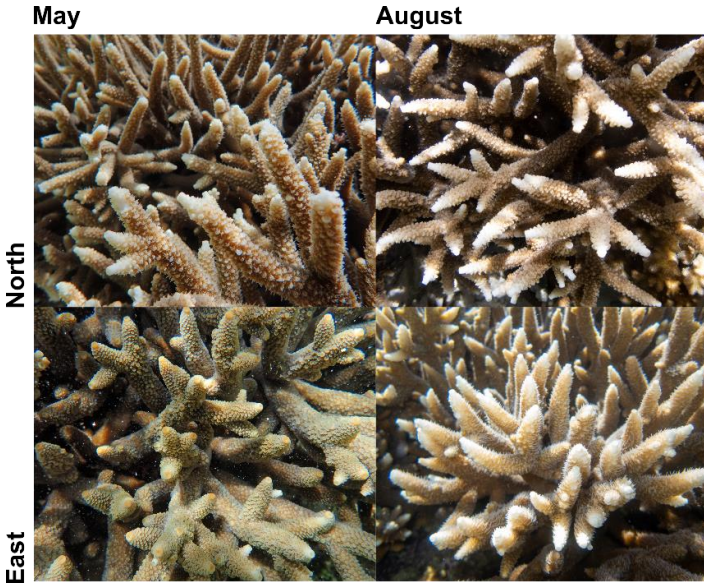


**Figure 2.8:** Colonies in different sites demonstrated different levels of pigmentation not only from each other, but also across seasons, as demonstrated by repeated photographs during May and August of the same colonies from the North and East sites.

***2.4.4 Phenotypic similarity between type profiles.*** Species of Symbiodiniaceae have been experimentally shown to have varying rates of plasticity to environmental change (Mansour et al.

2018); therefore, I predicted that the phenotypic fluctuations of a coral-associated Symbiodiniaceae assemblage would vary depending on the underlying diversity of its assemblage. The only site capable at beginning to disentangle this hypothesis was the North given its codominance of two ITS2 type profiles (Figure 2.4). The functional divergence of these two type profiles from nearshore to farshore indicates functional partitioning. However, upon assigning type profiles alongside their corresponding phenotypic data, I saw no significant pattern. Colonies from nearshore to farshore show some mild patterns of differential phenotypic characteristics, such as the higher abundance of photopigments in nearshore colonies versus farshore colonies (Figure 2.7). However, this variation is most likely not caused by the underlying ITS2 type profile. I successfully sampled two colonies within the same GPS-tagged plot with different type profiles. One plot showed type-profile specific differences; one did not (Figure 2.7). The colonies with different biodiversity related phenotypic characteristics showed no more variation than cohabitating colonies of identical type profiles (Figure 2.7). Therefore, neither the underlying diversity, nor cell density, explain the observed phenotypic. Instead, phenotypic variation is caused by phenotypic plasticity of individual Symbiodiniaceae cells.

## 2.5 Conclusions

As discussed in the introduction, previous research has not begun closing the gap in resolving how changes in phenotypic measurements are explained by adaptation (shifts or shuffles in symbiont) versus acclimation (phenotypic plasticity of individuals within an existing community). The results presented here suggest that Symbiodiniaceae phenotypic plasticity of individual cells is the primary mode of acclimation to mild environmental change, while changes in biodiversity are a form of long-term assemblage adaptation after acute selective events or in response to chronic environmental differences. Cell density did not vary within our data; therefore, I hypothesize

fluctuations in cell density only occur at the limits of individual acclimation or act as a rapid response to acute stressors and might be tightly associated with shifts in Symbiodiniaceae biodiversity. This work leaves many open-ended questions about the acclimation, adaptation, and function of Symbiodiniaceae and truly highlights the complexity and diversity of the coral holobiont acclimation and adaptation strategies; however, this is the first study, to my knowledge, that presents an island wide, repeated sampling with sample-paired, multi-level, quantification for the Symbiodiniaceae community, population, and individual cell.

Next steps should involve the complete quantification of these parameters through seasonal fluctuation. It is obvious that time contributes to variation, but with only two temporal samples, it is difficult to draw conclusions about acclimation strategies or physiological mechanisms that the cause observed variation reported in this study. Additionally, in-situ and ex-situ experimental work should aim to better understand type profile-associated functional differences. The heterogeneous biodiversity of our Northern colonies (Figure 2.7) could serve as an especially useful experimental reef system to pursue these questions. A simple reciprocal transplant between nearshore and farshore colonies within this site would be especially informative. Finally, the successful culturing followed by controlled ex-hospite physiological experiments would define the functional differences and resilience boundaries of Guam's *Acropopra*-associated Symbiodiniaceae. Guam's *Acropora* populations have suffered horribly in the last 10 years (Raymundo et al. 2017; Raymundo et al. 2019) but continued work with this research as the foundation could allow us to predict populations that are especially resilient to future acute-stress events.

## 2.6 Acknowledgments

I wish to thank Colin Lock (University of Guam), Dr. Brett Taylor (University of Guam), Dr. Cheryl Ames (Tohoku University), Dr. Héloïse Rouzé (University of Guam), and Dr. Shinichiro

Maruyama (University of Tokyo) for providing their expertise and mentorship. I would also like to thank Marine Laboratory boat captain, Jonathan “Nanny” Perez, for assisting with field collections in Cocos Lagoon, and the Ritidian Eco Beach Resort for allowing land access to the pristine reef flats of Urunao. Wave data was provided by the Pacific Islands Ocean Observing System (PacIOOS) (www.pacioos.org), which is a part of the U.S. Integrated Ocean Observing System (IOOS), funded in part by National Oceanic and Atmospheric Administration (NOAA) Awards #NA16NOS0120024 and #NA21NOS0120091. Guam NSF EPSCoR directly supported this work through National Science Foundation award OIA-1946352.

## 2.7 References


Aktas C (2020) haplotypes: Manipulating DNA Sequences and Estimating Unambiguous Haplotype Network with Statistical Parsimony. R package version 1.1.2.

Anthony CJ, Lock CC, Bentlage B (2022) High-throughput physiological profiling of endosymbiotic dinoflagellates (Symbiodiniaceae) using flow cytometry. bioRxiv. https://doi.org/10.1101/2022.12.06.519248

Baird AH, Guest JR, Willis BL (2009) Systematic and biogeographical patterns in the reproductive biology of scleractinian corals. Annu Rev Ecol Evol Syst 40:551-571. https://doi.org/10.1146/annurev.ecolsys.110308.120220

Baker A (2001) Reef corals bleach to survive change. Nature 411: 765-766. https://doi.org/10.1038/35081151

Baker AC (2003) Flexibility and specificity in coral-algal symbiosis: Diversity, ecology, and biogeography of *Symbiodinium*. Annu Rev Ecol Evol Syst 34:661–689. https://doi.org/10.1146/annurev.ecolsys.34.011802.132417

Baker AC, Starger CJ, McClanahan TR, Glynn PW (2004) Corals' adaptive response to climate change. Nature 430:741. https://doi.org/10.1038/430741a

Baker DM, Andras JP, Jordán-Garza, AG, Fogel ML (2013) Nitrate competition in a coral symbiosis varies with temperature among *Symbiodinium* clades. ISME J 7:1248–1251. https://doi.org/10.1038/ismej.2013.12

Baker DM, Freeman CJ, Wong JCY, Fogel ML, Knowlton N (2018) Climate change promotes parasitism in a coral symbiosis. ISME J 12:921-930. https://doi.org/10.1038/s41396-018-0046-8

Berkelmans R, van Oppen MJH (2006) The role of zooxanthellae in the thermal tolerance of corals: A ‘nugget of hope’ for coral reefs in an era of climate change. Proc R Soc B: Biol Sci 273:2305-12.

Brook G (1891) Descriptions of new species of *Madrepora* in the collections of the British Museum. Annals and Magazine of Natural History 8:458-471.

Brown B (1997) Coral bleaching: causes and consequences. Coral Reefs 16:S129–S138. https://doi.org/10.1007/s003380050249

Brown BE, Dunne RP, Ambarsari I, Le Tissier MDA, Satapoomin U (1999) Seasonal fluctuations in environmental factors and variations in symbiotic algae and chlorophyll pigments in four Indo-Pacific coral species. Mar Ecol Prog Ser 191:53-69.

Buddemeier RW, Fautin DG (1993) Coral bleaching as an adaptive mechanism: A testable hypothesis. BioScience 43(5):320-326. https://doi.org/10.2307/1312064

Camp EF, Edmondson J, Doheny A, Rumney J, Grima AJ, Huete A, Suggett DJ (2019) Mangrove lagoons of the Great Barrier Reef support coral populations persisting under extreme environmental conditions. Mar Ecol Prog Ser 625:1-14. https://doi.org/10.3354/meps13073

Castresana J (2000) Selection of conserved blocks from multiple alignments for their use in phylogenetic analysis. Mol Biol Evol 17:540-552.

Cignoni P, Callieri M, Corsini M, Dellepiane M, Ganovelli F, Ranzuglia G (2008) MeshLab: an Open-Source Mesh Processing Tool. Sixth Eurographics Italian Chapter Conference 129-136. https://doi.org/10.2312/LocalChapterEvents/ItalChap/ItalianChapConf2008/129-136

Cooper ED, Bentlage B, Gibbons TR, Bachvaroff TR, Delwiche CF (2014) Metatranscriptome profiling of a harmful algal bloom. Harmful Algae 37:75-83. https://doi.org/10.1016/j.hal.2014.04.016

Cooper TF, Ulstrup KE, Dandan SS, Heyward AJ, Kuhl M, Muirhead A, O'Leary RA, Ziersen BEF, van Oppen MJH (2010) Niche specialization of reef-building corals in the mesophotic zone: metabolic trade-offs between divergent *Symbiodinium* types. Proc R Soc B: Biol Sci 278(1713):1840-1850. https://doi.org/10.1098/rspb.2010.2321

Cunning R, Baker AC (2012) Excess algal symbionts increase the susceptibility of reef corals to bleaching. Nature Climate Change 3:259-262. https://doi.org/10.1038/nclimate1711

Dennison WC, Barnes DJ (1988) Effect of water motion on coral photosynthesis and calcification. J Exp Mar Biol Ecol 115:67–71. https://doi.org/10.1016/0022-0981(88)90190-6

Eckert RJ, Reaume AM, Sturm AB, Studivan MS, Voss JD (2020) Depth Influences Symbiodiniaceae Associations Among *Montastraea cavernosa* Corals on the Belize Barrier Reef. Front Microbiol 11:518.

Ezzat L, Fine M, Maguer JF, Grover R, Ferrier-Pagès C (2017) Carbon and nitrogen acquisition in shallow and deep holobionts of the scleractinian coral *S. pistillata*. Front Mar Sci 4:102. https://doi.org/10.3389/fmars.2017.00102

Fabricius KE, Mieog JC, Colin PL, Idip D, van Oppen MJH (2004) Identity and diversity of coral endosymbionts (zooxanthellae) from three Palauan reefs with contrasting bleaching, temperature and shading histories. Mol Ecol 13:2445-2458. https://doi.org/10.1111/j.1365-294X.2004.02230.x

Falkowski PG, Dubinsky Z, Muscatine L, Porter JW (1984) Light and Bioenergetics of a Symbiotic Coral. BioScience 34(11):705-709. https://doi.org/10.2307/1309663

Finelli CM, Helmuth BST, Pentcheff ND, Wethey DS (2006) Water flow influences oxygen transport and photosynthetic efficiency in corals. Coral Reefs 25(1):47–57. https://doi.org/10.1007/s00338-005-0055-8

Fitt WK, McFarland FK, Warner ME, Chilcoat GC (2000) Seasonal patterns of tissue biomass and densities of symbiotic dinoflagellates in reef corals and relation to coral bleaching. Limnol Oceanogr 3. https://doi.org/10.4319/lo.2000.45.3.0677

Frade PR, De Jongh F, Vermeulen F, Van Bleijswijk J, Bak RPM (2008) Variation in symbiont distribution between closely related coral species over large depth ranges. Mol Ecol 17:691–703.

Friedrich S, Konietshke F, Pauly M (2022) MANOVA.RM: Resampling-Based Analysis of Multivariate Data and Repeated Measures Designs. R package version 0.5.3.

Friedrich S, Konietshke F, Pauly M (2019) Resampling-Based Analysis of Multivariate Data and Repeated Measures Designs with the R Package MANOVA.RM. R J 11(2):380-400. https://doi.org/10.32614/RJ-2019-051

Fujise L, Nitschke MR, Frommlet JC, Serôdio J, Woodcock S, Ralph PJ, Suggett DJ (2018) Cell Cycle Dynamics of Cultured Coral Endosymbiotic Microalgae (Symbiodinium) Across Different Types (Species) Under Alternate Light and Temperature Conditions. J Eukaryot Microbiol 65(4):505–517. https://doi.org/10.1111/jeu.12497

Gates RD, Ainsworth TD (2011) The nature and taxonomic composition of coral symbiomes as drivers of performance limits in scleractinian corals. J Exp Mar Biol Ecol 408:94-101.

Gault JA, Bentlage B, Huang D, Kerr, AM (2021) Lineage-specific variation in the evolutionary stability of coral photosymbiosis. Sci Adv 7:eabh4243. https://doi.org/10.1126/sciadv.abh4243

Goulet TL (2006) Most corals may not change their symbionts. Mar Ecol Prog Ser 321:1-7. https://doi.org/3354/meps321001

Guoy M, Tannier E, Comte N, Parsons DP (2020) Seaview Version 5: A Multiplatform Software for Multiple Sequence Alignment, Molecular Phylogenetic Analyses, and Tree Reconciliation. In Multiple Sequence Alignment. Katoh, K. (ed). Methods in Molecular Biology, vol 2231. Humana, New York, New York. https://doi.org/10.1007/978-1-0716-1036-7_15

Hennige SJ, Smith DJ, Perkins R, Consalvey M, Paterson DM, Suggett DJ (2008) Photoacclimation, growth and distribution of massive coral species in clear and turbid waters. Mar Ecol Prog Ser 369:77-88. https://doi.org/10.3354/meps07612

Hooper DU, Chapin III FS, Ewel JJ, Hector A, Inchausti P, Lavorel S, Lawton JH, Lodge DM, Loreau M, Naeem S, Schmid B, Setala H, Symstad AJ, Vandermeer J, Wardle DA (2005) Effects of biodiversity on ecosystem functioning: A consensus of current knowledge. Ecol Monogr 75(1):3-35. https://doi.org/10.1890/04-0922

Howe-Kerr LI, Bachelot B, Wright RM, Kenkel CD, Bay LK, Correa AMS (2020) Symbiont community diversity is more variable in corals that respond poorly to stress. Glob Change Biol 26(4):2220-34. https://doi.org/10.1111/gcb.14999

Hughes TP, Barnes ML, Bellwood DR, Cinner JE, Cumming GS, Jackson JBC, Kleypas J, Kleypas J, van de Leemput, IA, Lough JM, Morrison TH, Palumbi SR, van Nes EH, Scheffer M (2017) Coral reefs in the Anthropocene. Nature 546:82–90. https://doi.org/10.1038/nature22901

Hume BCC, Ziegler M, Poulain J, Pochon X, Romac S, Boissin E, de Vargas C, Planes S, Wincker P, Voolstra CR (2018) An improved primer set and amplification protocol with

increased specificity and sensitivity targeting the *Symbiodinium* ITS2 region. PeerJ 6:e4816. https://doi.org/10.7717/peerj.4816

Hume BCC, Smith EG, Ziegler M, Warrington HJM, Burt JA, LaJeunesse TC, Wiedenmann J, Voolstra C (2019) SymPortal: A novel analytical framework and platform for coral algal symbiont next-generation sequencing ITS2 profiling. Mol Ecol Resour 19(4):1063-1080. https://doi.org/10.1111/1755-0998.13004

Iglesias-Prieto R, Beltrán VH, LaJeunesse TC, Reyes-Bonilla H, Thomé PE (2004) Different algal symbionts explain the vertical distribution of dominant reef corals in the eastern Pacific. Proc R Soc B: Biol Sci 271: 1757–1763.

Johnsen G, Samset O, Granskog L, Sakshaug E (1994) In vivo absorpition characteristics in 10 classes of bloom-forming phytoplankton: taxonomic characteristics and responses to photoadaptation by means of discriminant and HPLC analysis. Mar Ecol Prog Ser 105(1/2):149-157.

Jones AM, Berkelmans R, van Oppen MJH, Mieog JC, Sinclair W (2008) A community change in the algal endosymbionts of a scleractinian coral following a natural bleaching event: field evidence of acclimatisation. Proc Royal Soc B 275:1359–1365. https://doi.org/10.1098/rspb.2008.0069

Jones RJ, Yellowlees D (1997) Regulation and control of intracellular algae (= zooxanthellae) in hard corals. Philos Trans R Soc Lond B Biol Sci 352(1352):457-468. https://doi.org/10.1098/rstb.1997.0033

Karim W, Nakaema S, Hidaka M (2015) Temperature effects on the growth rates and photosynthetic activities of *Symbiodinium* cells. J Mar Sci Eng 3(2):368-381. https://doi.org/10.3390/jmse3020368

Kassambara, A (2020) ggpubr: 'ggplot2' Based Publication Ready Plots. R package version 0.4.0.

Katoh K, Standley DM (2013) MAFFT multiple sequence alignment software version 7: improvements in performance and usability. Mol Biol Evol 30(4):772–780.

Keshavmurthy S, Meng P-J, Wang J-T, Kuo C-Y, Yang S-Y, Hsu C-M, Gan C-H, Dai C-F, Chen CA (2014) Can resistant coral *Symbiodinium* associations enable coral communities to survive climate change? A study of a site exposed to long-term hot water input. Peer J 2:e327.

Krediet CJ, DeNofrio JC, Caruso C, Burriesci MS, Cella K, Pringle JR (2015) Rapid, Precise, and Accurate Counts of *Symbiodinium* Cells Using the Guava Flow Cytometer, and a Comparison to Other Methods. PLOS ONE 10(8):e0135725. https://doi.org/10.1371/journal.pone.0135725

LaJeunesse TC, Parkinson JE, Gabrielson PW, Jeong HJ, Reimer JD, Voolstra CR, Santos SR (2018) Systematic revision of Symbiodiniaceae highlights the antiquity and diversity of coral endosymbionts. Curr Biol. 28:2570–80. https://doi.org/10.1016/j.cub.2018.07.008

LaJeunesse TC, Pettay DT, Sampayo EM, Phongsuwan N, Brown B, Obura DO, Hoegh-Guldberg O, Fitt WK (2010) Long-standing environmental conditions, geographic isolation and host–symbiont specificity influence the relative ecological dominance and genetic diversification of coral endosymbionts in the genus *Symbiodinium*. J Biogeogr 37:785-800. https://doi.org/10.1111/j.1365-2699.2010.02273.x

Lajeunesse TC, Smith RT, Finney J, Oxenford H (2009) Outbreak and persistence of opportunistic symbiotic dinoflagellates during the 2005 Caribbean mass coral ‘bleaching’ event. Proc R Soc B: Biol Sci 276(1676):4139–4148. https://doi.org/10.1098/rspb.2009.1405

Lee CS, Yeo YSW, Sin TM (2012) Bleaching response of Symbiodinium (zooxanthellae): Determination by flow cytometry. Cytom Part A 81A(10):888-895. https://doi.org/10.1002/cyto.a.22111

Lesser MP (1996) Elevated temperatures and ultraviolet radiation cause oxidative stress and inhibit photosynthesis in symbiotic dinoflagellates. Limnol Oceanog 41:271–283.

Lesser MP, Slatter M, Stat M, Ojimi M, Gates RD, Grottoli A (2010) Photoacclimatization by the coral *Montastraea cavernosa* in the mesophotic zone: light, food, and genetics. Ecology 91:990-1003. https://doi.org/10.1890/09-0313.1

Liu G, Eakin CM, Chen M, Kumar A, De La Cour JL, Heron SF, Geiger EF, Skirving WJ, Tirak KV, Strong AE (2018) Predicting heat stress to inform reef management: NOAA Coral Reef Watch's 4-Month Coral Bleaching Outlook. Front Mar Sci 5:57. https://doi.org/10.3389/fmars.2018.00057

Lyndby NH, Kühl M, Wangpraseurt D (2016) Heat generation and light scattering of green fluorescent protein-like pigments in coral tissue. Sci Rep 6:26599. https://doi.org/10.1038/srep26599

Mangiafico S (2023) _rcompanion: Functions to Support Extension Education Program Evaluation_. R package version 2.4.21.

Mansour JS, Pollock FJ, Díaz-Almeyda E, Iglesias-Prieto R, Medina M (2018) Intra- and interspecific variation and phenotypic plasticity in thylakoid membrane properties across two *Symbiodinium* clades. Coral Reefs 37:81-850. https://doi.org/10.1007/s00338-018-1710-1

Martinez Arbizu P (2017) pairwiseAdonis: Pairwise Multilevel Comparison using Adonis. R package version 0.4.

Mass T, Einbinder S, Brokovich E, Shashar N, Vago R, Erez J, Dubinsky Z (2007) Photoacclimation of *Stylophora pistillata* to light extremes: metabolism and calcification. Mar Ecol Prog Ser 334:93-102. https://doi.org/10.3354/meps334093

Matthews JL, Crowder CM, Oakley CA, Davy SK (2017) Optimal nutrient exchange and immune responses operate in partner specificity in the cnidarian-dinoflagellate symbiosis. Proc Natl Acad Sci. 114:13194–13199. https://doi.org/10.1073/pnas.1710733114

Menne MJ, Durre I, Vose RS, Gleason BE, Houston TG (2012a) An overview of the Global Historical Climatology Network-Daily Database. J Atmos Ocean Technol 29:897-910. https://doi.org/10.1175/JTECH-D-11-00103.1

Menne MJ, Durre I, Korzeniewski B, McNeal S, Thomas K, Yin X, Anthony S, Ray R, Vose RS, Gleason BE, Houston TG (2012b) Global Historical Climatology Network - Daily (GHCN-Daily), Version 3.12. NOAA National Climatic Data Center http://doi.org/10.7289/V5D21VHZ [2022-04-15]

Mieog JC, Olsen JL, Berkelmans R, Bleuler-Martinez SA, Willis BL, van Oppen MJH (2009) The roles and interactions of symbiont, host and environment in defining coral fitness. PLOS ONE 4(7):e6364. https://doi.org/10.1371/journal.pone.0006364

Morris LA, Voolstra CR, Quigley KM, Bourne DG, Bay LK (2019) Nutrient Availability and Metabolism Affect the Stability of Coral-Symbiodiniaceae Symbioses. Trends Microbiol 27(8):678-689. https://doi.org/10.1016/j.tim.2019.03.004

Mullaney PF, Van Dilla MA, Coulter JR, Dean PN (1969) Cell sizing: a light scattering photometer for rapid volume determination. Rev Sci Instrum 40:1029-1032. https://doi.org/10.1063/1.1684143

Muscatine L, Falkowski PG, Porter JW, Dubinsky Z (1984) Fate of photosynthetic fixed carbon in light- and shade-adapted colonies of the symbiotic coral *Stylophora pistillata*. Proc R Soc Lond B. 222:181–202. https://doi.org/10.1098/rspb.1984.0058

Nitschke MR, Gardener SG, Goyen S, Fujise L, Camp EF, Ralph PJ, Suggett DJ (2018) Utility of Photochemical traits as Diagnostics of Thermal Tolerance amongst Great Barrier Reef Corals. Front Mar Sci 5:45. https://doi.org/10.3389/fmars.2018.00045

NOAA Coral Reef Watch (2019, updated daily) NOAA Coral Reef Watch Version 3.1 Daily 5km Satellite Regional Virtual Station Time Series Data for Guam, Jan. 1, 2021-Jan. 1, 2022. College Park, Maryland, USA: NOAA Coral Reef Watch. Data set accessed 2021-02-11 at https://coralreefwatch.noaa.gov/product/vs/data.php.

Oakley CA, Schmidt GW, Hopkinson BM (2014) Thermal responses of *Symbiodinium* photosynthetic carbon assimilation. Coral Reefs 33:501–512. https://doi.org/10.1007/s00338-014-1130-9

Ogle DH, Doll JC, Wheeler P, Dinno A (2022) FSA: Fisheries Stock Analysis. R package version 0.9.3.

Oken L (1815) Lehrbuch der Naturgeschichte. Dritter Theil: Zoologie. Erste Abtheilung: Fleischlose Thiere. xxviii + 842 pp. + xviii, 40 pls.

Oksanen J, Blanchet FG, Friendly M, Kindt R, Legendre P, Minchin PR, Wagner H (2019) Vegan: Community Ecology Package. R package version 2.5–6.

Oliveira CYB, Abreu JL, Santos EP Matos AP, Tribuzi G, Oliveira CDL,Veras BO, Bezerra RS, Müller MN, Gálvez AO (2022) Light induces peridinin and docosahexaenoic acid accumulation in the dinoflagellate *Durusdinium glynnii*. Appl Microbiol Biotechnol 106:6263–6276. https://doi.org/10.1007/s00253-022-12131-6

Oppen MJH van, McDonald BJ, Willis BL, Miller DJ (2001) The evolutionary history of the coral genus Acropora (Scleractinia, Cnidaria) based on a mitochondrial and a nuclear marker: reticulation, incomplete lineage sorting, or morphological convergence? Mol Biol Evol 18:1315–1329.

Palmer CV, Modi CK, Mydlarz LD (2009) Coral fluorescent proteins as antioxidants. PLOS ONE, 4(10):e7298. https://doi.org/10.1371/journal.pone.0007298

Parkinson JE, Coffroth MA, LaJeunesse TC (2015) New species of clade B *Symbiodinium* (Dinophyceae) from the greater Caribbean belong to different functional guilds: *S. aenigmaticum* sp. nov., S. antillogorgium sp. nov., *S. endomadracis* sp. nov., and *S. pseudominutum* sp. nov. J Phycol. 51(5):850–8. https://doi.org/10.1111/jpy.12340

Porter JW, Muscatine L, Dubinsky Z, Falkowski PG (1984) Primary production and photoadaptation in light- and shade-adapted colonies of the symbiotic coral, *Stylophora pistillata*. Proc R Soc B: Biol Sci 222(1227): 161-180. https://doi.org/10.1098/rspb.1984.0057

Price MN, Dehal PS, Arkin AP (2010) FastTree 2 – Approximately Maximum-Likelihood Trees for Large Alignments. PLOS ONE 5(3):e9490. https://doi.org/10.1371/journal.pone.0009490

Qin Z, Yu K, Chen B, Wang Y, Liang J, Luo W, Xu L, Huang X (2019) Diversity of Symbiodiniaceae in 15 coral species from the Southern South China Sea: Potential relationship with coral thermal adaptability. Front Microbiol 10:2343. https://doi.org/10.3389/fmicb.2019.02343

Ralph PJ, Gademann R (2005) Rapid light curves: A powerful tool to assess photosynthetic activity. Aquat Bot 82(3):222-237. https://doi.org/10.1016/j.aquabot.2005.02.006

Rambaut A (2018) FigTree v.1.4.4. http://tree.bio.ed.ac.uk/software/figtree/

Raymundo LJ, Burdick D, Hoot WC, Miller RM, Brown V, Reynolds T, Gault J, Idechong J, Fifer J, Williams A (2019) Successive bleaching events cause mass coral mortality in Guam, Micronesia. Coral Reefs, 38:677–700. https://doi.org/10.1007/s00338-019-01836-2

Raymundo LJ, Burdick D, Lapacek VA, Miller R, Brown V (2017) Anomalous temperatures and extreme tides: Guam staghorn *Acropora* succumb to a double threat. Mar Ecol Prog Ser 564:47-55. https://doi.org/10.3354/meps12005

R Core Team. (2021). R: A language and environment for statistical computing. R Foundation for Statistical Computing, Vienna, Austria. https://www.R-project.org/

Reichert J, Schellenberg J, Schubert P, Wilke T (2016) 3D scanning as a highly precise, reproducible, and minimally invasive method for surface area and volume measurements of scleractinian corals. Limnol Oceanogr Methods 14:518-526. https://doi.org/10.1002/lom3.10109

Rios D (2020) The population genetic structure of *Acropora pulchra* in Guam [Master's Thesis]. University of Guam.

Robison JD, Warner ME (2006) Differential impacts of photoacclimation and thermal stress on the photobiology of four different phylotypes of *Symbiodinium* (Pyrrhophyta). J Phycol 42(3):568-579. https://doi.org/10.1111/j.1529-8817.2006.00232.x

Roth MS (2014) The engine of the reef: photobiology of the coral-algal symbiosis. Front Microbiol 5. https://doi.org/10.3389/fmicb.2014.00422

Rouzé H, Lecellier G, Pochon X, Torda G, Berteaux-Lecellier V (2019) Unique quantitative Symbiodiniaceae signature of coral colonies revealed through spatio-temporal survey in Moorea. Sci Rep 9:7921. https://doi.org/10.1038/s41598-019-44017-5

Rouzé H, Lecellier GJ, Saulnier D, Planes S, Gueguen Y, Wirshing HH, Berteaux-Lecellier V (2017) An updated assessment of *Symbiodinium* spp. that associate with common scleractinian corals from Moorea (French Polynesia) reveals high diversity among background symbionts and a novel finding of clade B. PeerJ 5:e2856. https://doi.org/10.7717/peerj.2856

RStudio Team (2020) RStudio: Integrated Development for R. RStudio, PBC, Boston, MA. http://www.rstudio.com/

Sawall Y, Al-Sofyani A, Banguera-Hinestroza E, Voolstra CR (2014) Spatio-Temporal Analyses of *Symbiodinium* Physiology of the Coral *Pocillopora verrucosa* along Large-scale Nutrient and Temperature Gradients in the Red Sea. PLOS ONE 9(8):e103179. https://doi.org/10.1371/journal.pone.0103179

Shapiro HM (2003) Practical Flow Cytometry. 4th Edition. NJ: Wiley-Liss.

Silverstein RN, Cunning R, Baker AC (2017) Tenacious D: *Symbiodinium* in clade D remain in reef corals at both high and low temperature extremes despite impairment. J Exp Biol 220(7):1192–6. https://doi.org/10.1242/jeb.148239

Stat M, Morris E, Gates RD. (2008). Functional diversity in coral–dinoflagellate symbiosis. Proc Natl Acad Sci USA 105(27): 9256–61. https://doi.org/10.1073/pnas.0801328105

Steen HB (1980) Further developments of a microsocope-based flow cytometer: light scatter detection and excitation intensity compensation. Cytometry 1:26-31.

Suggett DJ, Kikuchi RKP, Oliveira MDM, Spanó S, Carvalho R, Smith DJ (2012) Photobiology of corals from Brazil's near-shore marginal reefs of Abrolhos. Mar Biol 159:1461-1473. https://doi.org/10.1007/s00227-012-1925-6

Suzuki G, Yamashita H, Kai S, Hayashibara T, Suzuki K, Iehisa Y, Okada W, Ando W, Komori T (2013) Early uptake of specific symbionts enhances the post-settlement survival of *Acropora* corals. Mar Ecol Prog Ser 494:149-158. https://doi.org/10.3354/meps10548

Swain TD, Lax S, Backman V, Marcelino LA (2020) Uncovering the role of Symbiodiniaceae assemblage composition and abundance in coral bleaching response by minimizing sampling and evolutionary biases. BMC Microbiol 20:124. https://doi.org/10.1186/s12866-020-01765-z

Szabó M, Wangpraseurt D, Tamburic B, Larkum AWD, Schreiber U, Suggett DJ, Kuhl M, Ralph PJ (2014) Effective light absorption and absolute electron transport rates in the coral *Pocillopora damicornis.* Plant Phys Biochem 83:159-167. https://doi.org/10.1016/j.plaphy.2014.07.015

Thornhill DJ, Lewis AM, Wham DC, LaJeunesse TC (2014) Host-specialist lineages dominate the adaptive radiation of reef coral endosymbionts. Evolution. 68(2):352–67. https://doi.org/10.1111/evo.12270

Tzur A, Moore JK, Jorgensen P, Shapiro HM, Kirschner MW (2011) Optimizing optical flow cytometry for cell volume-based sorting and analysis. PLOS ONE 6(1):e16053. https://doi.org/10.1371/journal.pone.0016053

Ulstrup KE, Hill R, van Oppen MJH, Larkum AWD, Ralph PJ (2008) Seasonal variation in the photo-physiology of homogeneous and heterogeneous *Symbiodinium* consortia in two scleractinian corals. Mar Ecol Prog Ser 361:139-150. https://doi.org/10.3354/meps07360

Venn AA, Wilson MA, Trapido-Rosenthal HG, Keely BJ, Douglas AE (2006) The impact of coral bleaching on the pigment profile of the symbiotic alga, *Symbiodinium*. Plant Cell Environ 29:2133-2142. https://doi.org/10.1111/j.1365-3040.2006.001587.x

Wallace CC (1999) Staghorn corals of the world: a revision of the coral genus *Acropora* (Scleractinia; Astrocoeniina; Acroporidae) worldwide, with emphasis on morphology, phylogeny and biogeography. CSIRO, Collingwood, Australia.

Wall C, Kaluhiokalani M, Popp B, Donahue M, Gates RD (2020) Divergent symbiont communities determine the physiology and nutrition of a reef coral across a light-availability gradient. ISME. 14(4):948-58. https://doi.org/10.1038/s41396-019-0570-1

Wangpraseurt D, Lichtenberg M, Jacques SL, Larkum AWD, Kühl M (2019) Optical properties of corals distort variable chlorophyll fluorescence measurements. Plant Phys 179(4):1608–1619. https://doi.org/10.1104/pp.18.01275

Warner ME, Fitt WK, Schmidt GW (1996) The effects of elevated temperature on the photsynthetic efficiency of zooxanthellae *in hospite* from four different species of reef coral: a novel approach. Plant Cell Environ 19(3):291-299.

Warner M, Chilcoat G, McFarland F, Fitt W (2002) Seasonal fluctuations in the photosynthetic capacity of photosystem II in symbiotic dinoflagellates in the Caribbean reef-building coral *Montastraea*. Mar Biol 141:31-38. https://doi.org/10.1007/s00227-002-0807-8

Watson JV (1991) Introduction to Flow Cytometry. Cambridge: Cambridge University Press.

Wickham H (2016) ggplot2: Elegant Graphics for Data Analysis. Springer New York. https://doi.org/10.1007/978-0-387-98141-3

Xiang T, Nelson W, Rodriguez J, Tolleter D, Grossman AR (2015) *Symbiodinium* transcriptome and global responses of cells to immediate changes in light intensity when grown under autotrophic or mixotrophic conditions. Plant J 82(1):67-80. https://doi.org/10.1111/tpj.12789

Zhu W, Liu X, Zhu M, Li X, Yin H, Huang J, Wang A, Li X (2022) Responses of Symbiodiniaceae Shuffling and Microbial Community Assembly in Thermally Stressed

*Acropora hyacinthus*. Front Microbiol 13:832081.

https://doi.org/10.3389/fmicb.2022.832081